SYNTHESIS AND CHARACTERIZATION OF ZINC OXIDE NANOPOWDER DOPED WITH COPPER BY MICROWAVE ASSISTED POLYOL METHOD

BY

ESAM GUNAID ABDO AL-NAHARI

A Thesis Presented to the

DEANSHIP OF GRADUATE STUDIES

KING FAHD UNIVERSITY OF PETROLEUM & MINERALS

DHAHRAN, SAUDI ARABIA

In Partial Fulfillment of the

Requirements for the Degree of

MASTER OF SCIENCE

In

Physics

May 2012

KING FAHD UNIVERSITY OF PETROLEUM & MINERALS
DHAHRAN 31261, SAUDI ARABIA

DEANSHIP OF GRADUATE STUDIES

This thesis, written by **ESAM GUNAID ABDO ALNAHARI** under the direction of his thesis advisor and approved by his thesis committee, has been presented to and accepted by the Dean of Graduate Studies, in partial fulfillment of the requirements for the degree of **MASTER OF SCIENCE IN PHYSICS.**

Thesis Committee

Dr. Saleh I. Al-Quraishi (Chairman)

Dr. Zain H. Yamani (Member)

Dr. Mohammed Al-Daous (Member)

Prof. Khalil A. Ziq (Member)

Dr. Fatah Z. Khiari (Member)

Dr. Abdulaziz Al-Jalal
(Department Chairman)

Dr. Salam A. Zummo
(Dean of Graduate Studies)

30/5/12

Date:

DEDICATION

I dedicate this dissertation with all of my love to

my parents, my family and my brothers.

ACKNOWLEDGMENT

First and foremost thanks to Allah Almighty who gave me strength, patience and ability to accomplish this work.

Acknowledgment is due to King Fahd University of Petroleum & minerals for supporting this work.

I also would like to thank Al-Hodeidah University, which gave me the opportunity for completing my M.Sc. degree in KFUPM.

I would like to express my appreciation to my thesis advisor Dr. Saleh I. Al-Quraishi for his guidance and patience through thesis, his continuous support and his encouragement. As I also wish to thank the committee members Dr. Zain H. Yamani, Dr. Mohammed Al-Daous , Prof. Khalil A. Ziq and Dr. Fatah Z. Khiari for their constant support and cooperation.

Thanks are due to the Chairman of the Physics Department for providing all available facilities. Particular thanks go to Dr. Abbas Hakeem for FESEM images and Mr. Mohammed Al-Saeed for analyzing our samples by XRD and XPS. I am also grateful to all people, who helped and encouraged me during this work.

TABLE OF CONTENTS

LIST OF TABLES

LIST OF FIGURES

THESIS ABSTRACT

Name: Esam Gunaid Abdo Al-Nahari

Title: Synthesis and Characterization of Zinc Oxide Nanopowder Doped with Copper by Microwave assisted Polyol Method

Major Field: Physics

Date of Degree: May 2012

In this work, pure and Cu-doped ZnO samples ($Zn_{1-x}Cu_xO$, x=0, 0.02, 0.04, 0.06, 0.08, 0.10, 0.12, 0.14) have been prepared using microwave assisted polyol method from zinc and copper acetates dissolved into diethylene glycol (DEG) at 180 °C and 200 °C.

The structure, morphology and optical properties of synthesized pure and doped samples have been characterized by X-Ray Diffraction (XRD), X-Ray Photoelectron Spectroscopy (XPS), Field Emission Scanning Electron Microscopy (FESEM), and UV-visible light spectroscopy (UV-vis).

XRD results showed that pure ZnO and Cu-doped ZnO synthesized by microwave assisted polyol method at 180 °C and 200 °C have a hexagonal structure. The results showed that the grain size increases with increasing temperature whereas it decreases with increasing Cu doping concentration. In the present investigation we did not observe any noticeable change in the lattice parameters of Cu- doped ZnO for all synthesized samples.

X-Ray Photoelectron Spectroscopy (XPS) technique has provided elemental and chemical information of Cu-doped ZnO samples and the results emphasized the presence of Cu^{+2} within Zn^{+2} crystals.

FESEM investigation of pure ZnO and Cu-doped ZnO synthesized by microwave assisted polyol method at 180ºC and 200ºC showed spherical primary particles consisting of agglomerated nanoparticles. The samples synthesized at 180ºC had spherical shape more regularity than those samples synthesized at 200ºC.

EDX spectra clearly confirm the chemical purity of the investigated samples. The chemical composition of samples indicates two components; Zn and O for pure samples whereas three components: Zn, Cu and O for doped ZnO samples.

The effect of doping on the band gap of ZnO was studied by UV -visible diffuse reflectance spectroscopy. The results showed that the energy band gap of synthesized ZnO decreases very slightly from 3.29 to 3.26 eV with increasing Cu doping concentration within the ZnO samples.

MASTER OF SCIENCE DEGREE

KING FAHD UNIVERSITY OF PETROLEUM AND MINERALS

DHAHRAN, SAUDI ARABIA

May 2012

ملـخص الرســالة

الاســـــــــــم: عصام جنيد عبده النهاري

عنوان الرسالة: إنتاج وفحص مادة أكسيد الزنك المطعمة بالنحاس ذات البنية النانوية بواسطة طريقة البوليول بمساعدة الميكروويف.

التخصـــــــص: فيزياء

تاريخ التخـرج: مايو 2012

في هذا العمل انتجت عينات من مادة أكسيد الزنك النانوية المطعمة بنسب مختلفة من النحاس باستخدام طريقة البوليول ومساعدة الميكروويف عند درجتى الحرارة 180 و 200 مئوية. وقد فحصت خصائص هذه العينات المنتجة بعدة أجهزة مثل جهاز حيود الأشعة السينية (XRD)، وجهاز مطياف الإلكترون الضوئي (XPS)، والمجهر الإلكتروني الماسح (FESEM)، لقد أظهرت نتائج XRD أن التركيب البلوري السداسي لأكسيد الزنك لم يتغير بسبب عملية التطعيم . وكما أظهرت أيضا أن هناك زيادة تنشأ في حجم الجسيمات النانوية الدقيقة المكونة لأكسيد الزنك مع زيادة درجة حرارة الإنتاج في حين أن ارتفاع تركيزالتطعيم بالنحاس يقلل من حجم هذه الجسيمات النانوية الدقيقة. أما بالنسبة لأبعاد بلورة أكسيد الزنك فلم تعاني من أي تغيربسبب التطعيم بمادة النحاس نظراً لتقارب نصف القطر الايوني لأكسيد الزنك وأكسيد النحاسيك

. وقد شخص جهاز مطياف الإلكترون الضوئي (XPS) بعض العينات المنتجة المطعمة بالنحاس مؤكدة وجود أيونات Cu^{+2} ضمن الشبكة البلورية لأكسيد الزنك. كما أن المجهر الإلكتروني الماسح (FESEM) أعطى صوراً لشكل جسيمات مادة أكسيد الزنك النقية والمطعمة بالنحاس حيث لم يتغير الشكل, حيث لوحظ وجود حبيبات كروية كبيرة متشكلة من جسيمات نانوية دقيقة. وقد اتخذت الحبيبات الكبيرة الشكل الكروي الذي ظهر أكثر تجانساً وانتظاماً عند درجة الحرارة 180 مئوية. وأظهرت نتائج جهاز مطياف تشتيت طاقة الأشعة السينية(EDX) نقاوة العينات المنتجة من أي شوائب أو مواد أخرى يمكن أن تتواجد ضمن العينات. وكما تمت دراسة تأثير التطعيم بالنحاس على طاقة فجوة الربط لأكسيد الزنك بين حزمة التوصيل وحزمة التكافؤ، وأظهرت النتائج أن طاقة فجوة الربط لأكسيد الزنك تناقصت بشكل ضئيل جداً من 3.29 إلى 3.26 إلكترون فولت.

ماجستير العلوم

جامعة الملك فهد للبترول والمعادن

الظهران – المملكة العربية السعودية

مايو 2012

CHAPTER 1

INTRODUCTION

1.1. INTRODUCTION

The term “nanoparticles” is used to define ultrafine particles that cover a size range between 1 to 100 nanometers. Nanometer is 10^{-9} meter, or one billionth of a meter. Nanoparticles acquire unique properties that differ from those of bulk materials. This is due to four factors[1]: the specific surface area of the material, the smallness of the size, the size dependent properties, and the high fraction of atoms on the surface relative to those on the interior of the particle. Obviously, the specific surface area increases as the size of the particle decreases. This is very important in catalysis where large surface area is usually needed. Large surface area leads to an increase in the number of atoms situated at the surface of the nanoparticles. It represents contacting and interacting points among materials and has activity much more than those inside the material particles. The smallness of the nanoparticles increases its penetration ability through many barriers such as cells tissues and membranes. This property was utilized in many medical applications and many industries[1-2]. The size dependent properties are due to quantum effects that can be exhibited in materials at nanoscale sizes. It is responsible for absorption of light of a certain frequency and the development of discrete energy levels[1],[3]. Finally, the large number of surface atoms relative to the bulk atoms

increases the surface energy per unit volume. This, in turn, causes some changes in the particle's physical properties such as melting point and related properties.

Moreover, nanoparticles can be produced in various morphologies such as spheres, tubes, cylinders, disks and platelets which may have different chemical compositions. They can be composed of metals, metal oxides (inorganic nanoparticles) or organic materials such as polymers, etc [4].

1.2. SYNTHESIS METHODS

There are several techniques used for producing nanomaterials. These can be essentially divided into two categories according to the type of precursor materials used in the synthesis; methods using solid precursors and methods using liquid or vapor precursors. Each method is suitable for synthesizing specific nanostructured materials according to the needs and application fields [5].

1.2.1. Methods using solid precursors

1.2.1.1. Inert gas condensation

In this method, the solid precursor material is heated to evaporate into a background gas inside a sealed and evacuated chamber. Then, the vapor is mixed with a cold gas to reduce the temperature. Finally, the desired product is collected as powder. This method

is well suited for producing metal nanoparticles since many metals evaporated at reasonable rates at attainable temperatures. Oxides or other compounds of the evaporated material can be prepared by including a reactive gas, such as oxygen, in the cold gas stream[6-7].

1.2.1.2. Pulsed laser ablation

In this method the material is removed from the surface of a target by irradiating it with a high intensity laser beam focused onto the fixed or rotating target. The absorbed laser beam energy either produces plasma or just evaporates the material. The laser beam intensity is high enough to ablate small amounts of the surface of the target material. The produced material is either collected as powder or deposited on a substrate. This technique was used to produce thin films of a wide range of composition and a variety of nanomaterials[8- 9].

1.2.1.3. Sputtering

This technique is based on removal of atoms from a target due to bombardment by energetic ions. The target atoms that will be ionized become positive ions after losing some electrons. These ions are sputtered and controlled by different parameters such as: electrostatic voltage, pressure and target substrate distance [10].

1.2.1.4. Sparks discharge generation

The principle of this method depends on generating a spark discharge between two electrodes of precursor materials by a charged capacitor with a high voltage. Electrode material is evaporated by the spark. The final product is obtained by nucleation of the evaporated material. There are many advantages of this method such as synthesizing different nanomaterials by controlling the distance between electrodes, possibility of inserting an inert gas if needed and controlling the spark discharge frequency that controls the vaporization rate[11].

1.2.2. Methods using liquid or vapor precursors

1.2.2.1. Spray pyrolysis

In this method, the precursor solution is prepared and then atomized by a spraying system inside a reactor. The flow rate of the precursor solution is controlled by a constant pressure feed system. The droplets of precursor solution are evaporated into the rector. Finally, the new product is collected from the reactor as powders [12-13].

1.2.2.2. Laser pyrolysis

Nanoparticles can be fabricated by laser pyrolysis method. This method is based on absorption of laser radiation by the reactant materials. The reactant materials are evaporated in the presence of air or any gas such as oxygen to obtain the desirable

product. The product material is formed by nucleation and growth. The product is collected as powder[14–16].

1.2.2.3. Thermal plasma synthesis

This is another method for producing nanomaterials. Precursors are treated inside a thermal plasma reactor. Argon was used to generate the plasma torch. The precursors are injected continuously into the torch tail region by a carrier gas. The final product is formed and collected as powder [17-18].

1.2.2.4. Flame spray pyrolysis

The nanoparticles can be synthesized with the flame spray pyrolysis. The precursor materials are sprayed with a nozzle, surrounded and burnt by a flame in the presence of

a flow rate of oxygen and methane. The final material is collected with the aid of a filter connected to vacuum [19].

1.2.2.5. Low-temperature reactive synthesis

This method is used for synthesizing nanomaterials at low temperature. The precursor materials are separately dissolved in a suitable solvent. The solutions are continuously stirred at low temperature such as 70°C for a certain time. One of the solutions is slowly added to the other with continuous stirring forming final solution. The final solution is

centrifuged, washed several times with deionized water or ethanol and dried to obtain the desired nanopowder[20-21].

1.2.2.6. Chemical vapor synthesis

Chemical vapor synthesis (CVS) is another process that can be utilized for synthesizing nanomaterials. The reaction is achieved in a modular CVS reactor under suitable conditions. In such a process, the reactor is connected to precursor delivery units, reaction, heating, collecting zones and a pumping unit. One of the advantages of this technique is synthesis of wide range of nanomaterials[22-23].

1.2.2.7. Precipitation process

In this process, the precursor materials are slowly dissolved into a solvent material. Then, the solution is placed in a reactor vessel with vigorous stirring. The precipitate material is obtained, filtered and washed several times with deionized water.

Finally, the obtained powder is dried at low temperature and then calcined to high temperature [24-25].

1.2.2.8. Hydrothermal synthesis

Hydrothermal process is also one of the methods for synthesizing nanomaterials using liquid precursors. This process involves a chemical reaction of precursor materials in the presence of aqueous solvents at high temperature. In this process, the high temperature is

a significant factor for dissolving the precursor materials which cannot be dissolved in normal conditions. Then the solution is transferred into a Teflon-lined stainless steel autoclave and stirred. Then it is cooled down to room temperature, filtered, washed several times with distilled water or ethanol and dried at low temperature. The resultant is collected as a powder [26–28] .

1.2.2.9. Microwave assisted polyol method

This technique represents one of the promising techniques used for synthesizing nanomaterials. In this technique, a microwave oven is used as a source of heating the precursor material and polyol materials such as ethylene glycol (EG) or diethylene glycol (DEG) are used as solvents, reducing agents, and surfactants.

Microwave oven generates electromagnetic radiations that are absorbed by the sample in a short time. The electromagnetic radiations generate heat within the material.

This property is different from that in the conventional heating in which the heat transfers from the surface of material towards the inside.

The main advantages of this method are that it is a simple, fast and efficient technique. Moreover, microwave heating enhances the uniformity of the size distribution of the final product. The degree of nucleation of synthesized nanocrystalline materials using this method is controlled by the temperature, exposure time, and ratio of precursor material to solvent[29–32]. Last but not least, the precursor compounds such as hydroxides, oxides, nitrates, sulfates, and acetates can easily be used as dissolved or

suspended solutions in the polyol. In our work, this method was used for synthesizing pure and doped ZnO. Zinc Oxide (ZnO).

1.3. ZINC OXIDE (ZNO).

ZnO belongs to II-VI semiconductors materials. It has a direct band gap (E_g~3.37 eV), a large exciton binding energy (60 meV) and other unique piezoelectrical, electrical and optical properties [33]. As a result of these properties, ZnO has been utilized in many applications such as gas sensors, varistors, catalysis, etc…[4].

ZnO can be formed in nature on two structures, hexagonal wurtzite and cubic zincblende. The hexagonal wurtzite is common due to its high stability in normal conditions[34].

ZnO can be synthesized in several structures such as, nanotubes, nanoneedles, nanobelts, nanocombs, nanorods, nanorings, nanowire,etc…[34-35].

ZnO nanostructured material can be produced by different methods such as mechanical processing [7], hydrothermal process [36], sol–gel method [37], laser ablation method [38] spray pyrolysis method [13] and combustion method [39].

The Electrical, magnetic and optical properties of ZnO nanoparticles can be enhanced or modified by doping with transition metals such as Ag, Cu, Co, or Ni [40]. Doping ZnO with nitrogen converts ZnO from n-type to p-type semiconductor [41- 42].

In this work, the microwaves-assisted polyol method was used to synthesize pure and doped ZnO nanoparticles with copper. Predetermined amounts of zinc acetate and

copper acetate were mixed with diethylene glycol (DEG) solvent. The solution was stirred and then treated in domestic microwave that has been modified with a home-made temperature control system. The temperature, the concentration of the acetates and the exposure time was varied to study their effect on the synthesized nanostructure. At the end of this process, the precipitate was collected and washed, then centrifuged to remove the residues and dried.

1.4. IMPORTANCE OF THE TOPIC

The synthesis of Cu-doped ZnO is important for the following reasons:

- The synthesized material can be used in different applications such as photo-catalysis and gas sensing.
- Acquiring the know-how about microwave assisted polyol method will help in the establishment of material science lab for nanomaterials synthesis in physics department at KFUPM.
- Effects of doping ZnO with Cu might change the properties of ZnO such as lattice parameters, band gap energy, etc….

1.5. OBJECTIVES

The main objectives of this work are:

a. To build an external microwave power control circuit that enables us to control synthesis temperature.
b. To synthesize nanostructured pure ZnO and ZnO doped with copper, using microwave-assisted polyol method.
c. To characterize the synthesized materials using X-Ray Diffraction technique (XRD) and Scanning Electron Microscopy (SEM).
d. To study the effect of synthesis temperature on the size and the morphology of synthesized nanostructured materials.
e. To study the effect of concentration of zinc and copper acetates on the structure and the morphology of synthesized nanostructured materials.

CHAPTER 2

LITERATURE REVIEW

Zinc oxide (ZnO) is of great interest to many researchers due to its unique properties. Substantial efforts have been devoted to enhance or modify ZnO properties for different applications. Doping was one of the efforts that used the precursor materials as a way to improve the properties of ZnO. In this chapter we will review works that were applied to synthesize pure and doped ZnO.

Weiqin Ao et al. [43] reported that pure zinc oxide nanoparticles were synthesized with the mechanochemical reaction method followed by heat-treatment. The particle size of the ZnO nanoparticles ranged from 18 nm to 36 nm when synthesized between 400 °C and 800 °C.

It was reported by Yonghong Ni et al. [33] that the simple solution- combustion method was successful for synthesizing pure ZnO nanoparticles. They found that the ZnO has the wurtzite structure. UV–vis spectroscopy showed that an absorption peak was obtained at 374 nm.

Sul Lee et al.[44] synthesized ZnO nanoparticles with controlled shapes and sizes by a simple polyol method. In their work, they obtained two shapes; rod-shaped particles with an average major axis length of 114 ± 54 nm and minor axis length of 31 ± 10 nm and equiaxial particles with an average diameter of 34 ± 9 nm.

ZnO nanoparticles were synthesized by the solvothermal method [45]. XRD results revealed that ZnO phase was hexagonal. ZnO nanoparticles and nanorods were obtained using ethanol and diethylene glycol as solvents, respectively. ZnO nanorods prepared with ethanol had a diameter and a length of 8 ± 2 nm and 54 ± 11 nm, respectively. ZnO nanoparticles prepared with diethylene glycol had diameters of 68 ± 7 nm.

Ning Wang et al. [46] reported that the facile low temperature reaction was successful for synthesizing ZnO nanosheets. The precursor materials were dissolved in deionized water. XRD results indicated a hexagonal phase of ZnO. SEM and TEM images revealed that the morphology of the product was nanosheets. The thickness of ZnO nanosheets can be changed from 10-20 nm to 30-40 nm if the reaction temperature altered from 80 ºC to 180 ºC.

It was reported by Takao Tani et al. [47] that ZnO nanoparticles were fabricated by flame spray pyrolysis. The phase of ZnO nanoparticles was hexagonal and the average grain size was in a range of 10 to 20 nm.

Yoshie Ishikawa and his team[48] fabricated ZnO nanorods by pulsed laser ablation method in deionized water at different temperature with and without surfactants, lauryl dimethylaminoacetic acid (LDA) and cetyltrimethylammomium bromide (CTAB). The ZnO structure was hexagonal as revealed by XRD. The size of nanorods was around 500-600nm long and 200nm wide. LDA effect was clear in decreasing ZnO nanorods size whereas CTAB did not have any affect.

Kushal D.Bhatte et al.[49] synthesized ZnO nanoparticles using domestic microwave. Zinc acetate as precursor was dissolved in butanediol as solvent. The mixture was heated by microwave for 2 minutes. The product was centrifuged, washed with deionized water and alcohol several times then dried at 60 °C for 4 hours. XRD showed that the obtained phase was hexagonal and the average particle size was around 40 nm.

Xingyan Xu and Chuanbao Cao [50] reported the synthesis of single-phase $Zn_{1-x}Co_xO$ (x=0.02, 0.04) powders were synthesized by a simple co-precipitation technique. XRD results revealed that the Co-doped ZnO structure was a wurtzite. Authors found that the lattice parameters of ZnO powders decreased slightly when Zn was substituted with Co. The optical absorption spectra showed that the band gap decreases when the concentration of Co increased

M. Zheng and J. Wu [51] fabricated the nitrogen-doped ZnO nanocrystallite by self-assembly combustion technique (SAC). XRD results revealed that the phase of doped ZnO was hexagonal. In addition, the chemical analysis of the product was done by XPS, and it was found that there is an N–O bonding region in ZnO crystal lattice because of the nitrogen incorporation.

Mn-doped ZnO nanorods were synthesized by solvothermal route [52]. The morphological and structural properties of the doped ZnO were investigated by (High Resolution Transition Electron Microscopy) HRTEM and XRD. The results showed that

the morphology of the production was nanorod and the preferential growth direction was along the c-axis.

Hydrothermal method was used for producing ZnO doped with indium nanoparticles [53]. The growth of ZnO crystals had a plate-like form in the presence of In^{3+}. UV-visible spectrophotometer results showed that transmittance of ZnO crystals decreased due to doping with indium. The absorption edge red-shifted compared with undoped ZnO crystals. The resistivity of indium-doped ZnO crystals was lower than 0.015 Ω.cm at room temperature.

D.W. Zeng et al.[54] prepared Sb-doped ZnO nanoparticles with wurtzite structure by vapor condensation method from Zn–Sb alloy as precursor in the environment of Ar and O_2 gases. The average grain size was about 60 nm. XPS results showed that Sb was found within the ZnO crystal lattice. The doped Sb^{5+} ions led to a considerable increase of the optical reflectivity and electrical resistivity in comparison with the undoped ZnO nanoparticles.

ZnO nanoparticles doped with Cu, Mn and Fe were synthesized by solid state reaction method and co-precipitation method [55]. XRD, XRF and mapping analyses results showed that Zn was successfully substituted with Cu, Mn and Fe and all doped compounds were well crystallized.

Zhou Zhang et al. [56] had synthesized Cu-doped ZnO nanoneedles and nanonails by thermally evaporating Zn and $CuCl_2$ powders. XRD results showed that doped

nanostructured ZnO was hexagonal and the lattice parameters decreased because of the doping. Photoluminescence results showed that the band-edge UV emission and the broad green emission are red-shifted by about 7nm and 20nm, respectively.

K.G. Kanade et al. [57] fabricated ZnO nanoparticles doped with Cu in aqueous and organic reaction mediums. XRD showed that nanocrystalline ZnO was hexagonal. The average grain size was in the (40 nm –55 nm) range for organic mediated Cu-ZnO whereas it was in the (50nm – 85 nm) range for aqueous mediated ZnO. The copper was found in an oxide form located at the core of prismatic ZnO form with clear edges and faces.

In this work, doped zinc oxide with copper was synthesized by means of microwave assisted polyol method. Different techniques namely XRD, XPS, FESEM and UV-visible spectrophotometer were used to characterize the material.

CHAPTER 3

EXPERIMENTAL WORK

Microwave assisted polyol method is considered to be one of the best techniques used for synthesizing nanostructure metal oxides because it is fast, simple, energy efficient and can be used to synthesize a variety of doped metal oxide nanostructured powders[30].

3.1. APPARATUS

We used a domestic microwave oven [ULTRA, UT-9900] to carry out the synthesis reaction. The temperature was monitored by a home-made thermocouple which can be used inside the microwave cavity. The thermocouple was calibrated by a thermometer. A hole was opened on the upper side of the microwave to insert the thermocouple inside the beaker containing the reactant material. In addition to the built-in power control of the microwave, we added an electric circuit that enabled control of the power of the microwave externally thus giving control over the temperature of the solution at the desired value during the course of the synthesis experiment. A schematic diagram of the synthesis device is shown in Figure 3-1.

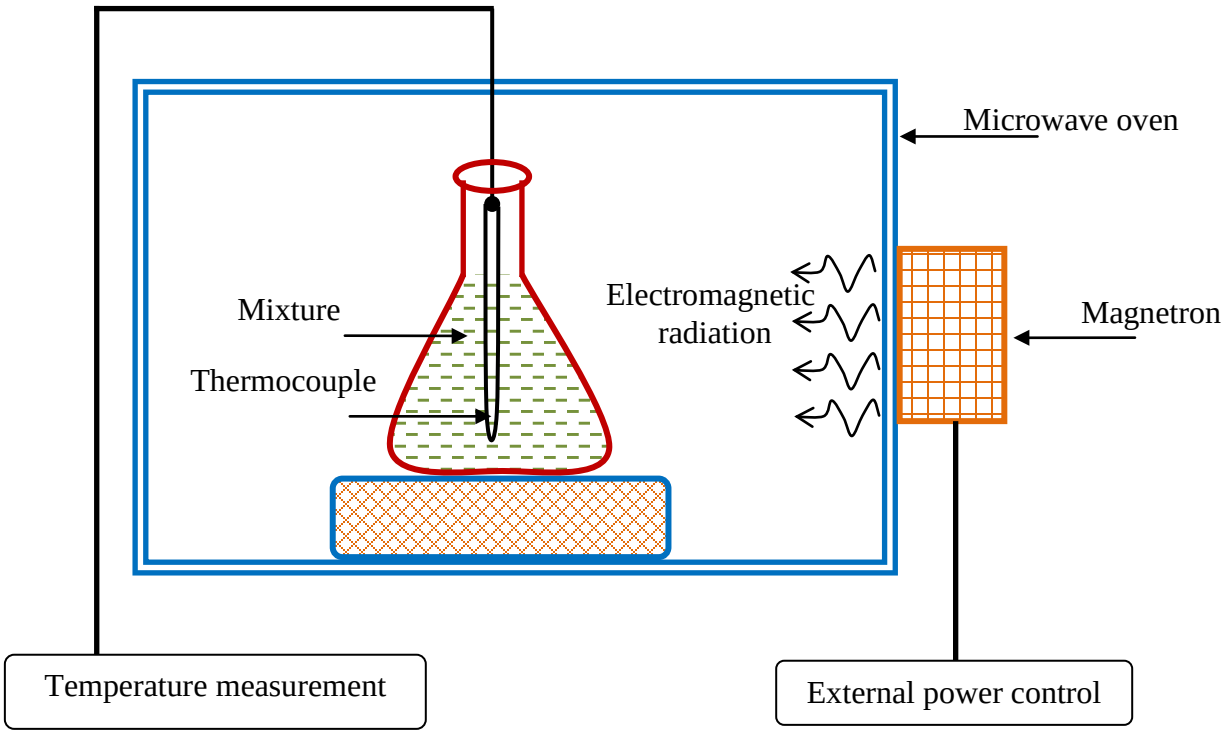

Figure 3-1 Schematic diagram of experimental synthesis set up

3.2. MATERIALS AND PROCEDURE

The precursor materials used in this work were zinc acetate $Zn(O_2CCH3)_2(H2O)_2$ [SIGMA-ALDRICH Pcode:100930197], and copper acetate $Cu(CH_3COO)_2$ [PANREAC cod. 141261] as dopant and diethylene glycol DEG was used as solvent and reducing agent. The used ratios, in gram, of zinc acetate to solvent DEG were 1, 2, 3 and 4 % of the total mixture. Also, the ratios of copper acetate to zinc acetate were 2, 4, 6, 8, 10, 12 and14%.

The precursor materials were weighted and added together to DEG. The mixture was heated at ~ 85 °C and stirred until the mixture became homogenous and clear. The solution was then cooled down to 35 °C, and transferred to a domestic microwave oven, where the reaction was conducted for 20 min. After 5 minutes the color of the solution changed from clear to white/creamy color indicating the formation of the oxides. At the end of the reaction time, the mixture was cooled down in cooled water to stop the reaction and the precipitates were collected by centrifugation and washed twice with ethanol to remove the residues. The final product was then dried in air for several hours and collected as powder. The samples were synthesized at temperatures of ~180 ºC and 200 ºC.

The synthesized Cu-doped ZnO samples had different colors about the white pure ZnO sample. These colors changed with increasing doping concentrations of Cu.

Figure 3-2 shows the conversion of ZnO color to several colors after its doping with Cu.

The Cu concentrations of 2% of precursor materials were measured by Inductively Coupled Plasma (ICP) technique and compared with the used Cu concentrations.

Table 3-1concentrations of Cu as used versus Cu concentrations measured by ICP technique for 2% of precursor materials

% of Cu concentration as used	% of Cu concentration measured by ICP
2	1.2
4	2.7
6	5.4
8	8.5
10	8.7
12	9.6
14	13.5

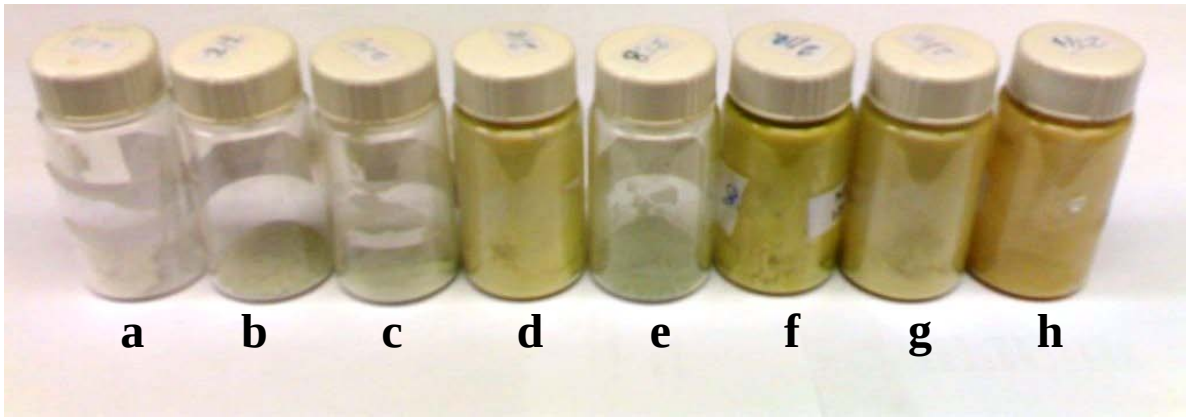

Figure 3-2 The synthesized samples of pure ZnO and Cu- doped ZnO (a) Pure (b) 2 % Cu (c) 4 % Cu (d) 6 % Cu (e) 8 % Cu (f) 10 % Cu (g) 12 % Cu (h) 14 % Cu

CHAPTER 4

CHARACTERIZATION TECHNIQUES

4.1. X-RAY DIFFRACTION

X-ray diffraction is one of the analytical techniques used for materials characterization such as phase identification, measurement of lattice parameters and grain size measurement. An x-ray diffractometer consists of an x-ray tube, a diffractometer assembly which controls the beam alignment as well as the position and orientation of the sample, and x-ray detector (see Figure4-1).

The x-rays used in the diffractometers must be monochromatic. X-rays are generated by excitation of K-radiation from a pure metal target and then filtering the beam by a foil which has the ability of absorbing the β-component of the K-radiation without any appreciable reduction in the intensity of α-component. The use of a nickel filter with a copper target is considered a good example for transmitting the Cu-K_α beam and blocking the Cu-K_β component[58-59].

When the x-rays strike a plane of atoms in the sample surface is either scattered or absorbed. The interactions of x-rays with the atoms of the sample material provide the structural information of its crystal lattice. The diffraction pattern yield depends on two factors, diffraction angles and diffracted beam intensities.

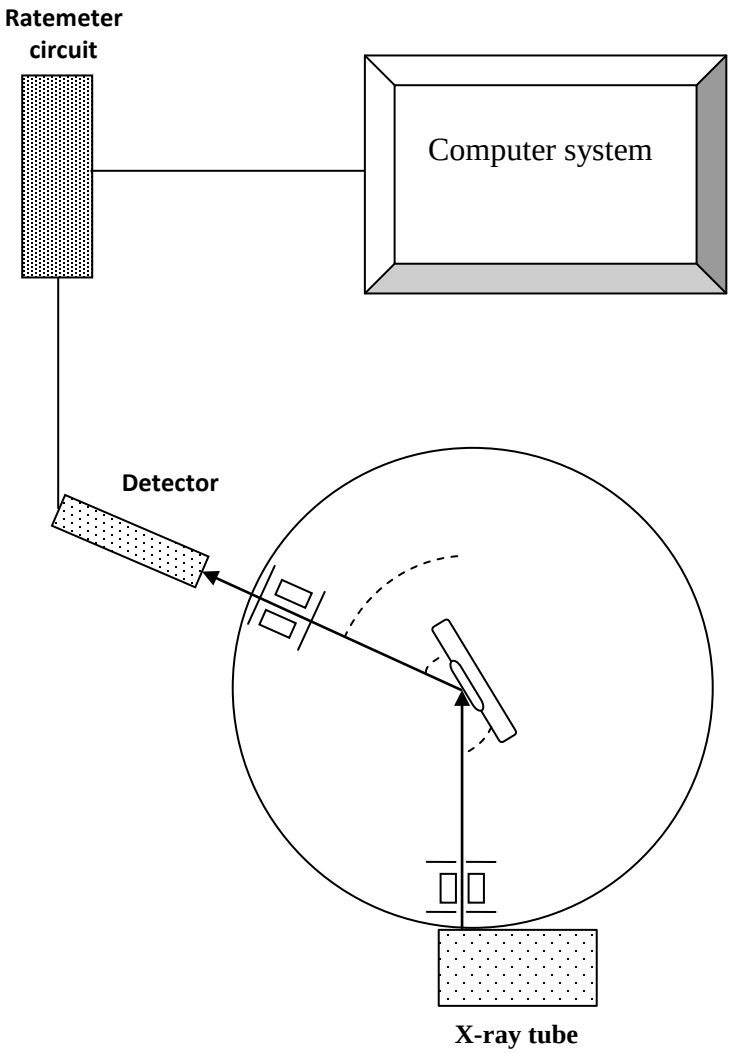

Figure 4-1 Schematic diagram representing an x-ray diffractometer.

The diffraction angles depend on the Bravais point lattice and the unit cell dimensions, while the diffracted intensities depend on the atomic numbers of the constituent atoms and their geometrical relationship with respect to the lattice points.

To obtain a diffraction pattern, the wavelengths of incident x-rays should be equal or less than interatomic spacing in the lattice. The diffraction pattern is given by Bragg's equation

$$n\,\lambda = 2d\,sin\theta_B$$

where *n* is an integer referring to the order of diffracted beam, λ is the wavelength of the radiation, *d* is the distance between the sequential planes of the crystal lattice, and θ is the angle that the incident beam makes with the lattice planes.

Figure 4-2 shows the diffraction of x-rays beam incident on lattice planes[58- 59]

For estimating grain size the Scherer's equation is used and is given by[60]:

$$g = \frac{0.9\ \lambda}{\beta cos\theta}$$

where g is the diameter of the grain size, λ is the wavelength of x-ray radiation source, $\beta \equiv \sqrt{\beta_m^2 - \beta_s^2}$ where β_m is the measured peak width and β_s is the instrumental peak width.

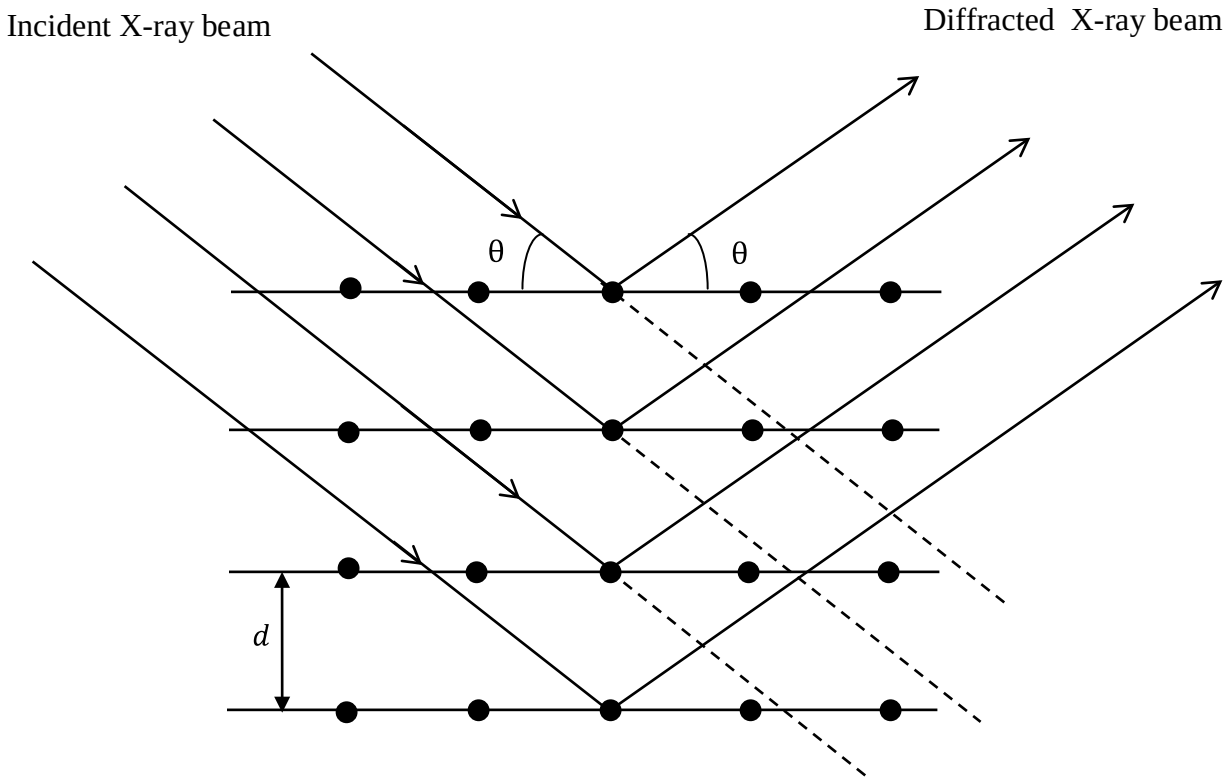

Figure 4-2 Diffraction of X-rays incident on lattice planes

In this thesis we were mostly concerned with the investigation of the crystalline structures, estimation of lattice parameters of ZnO doped Cu and particle (grain) size. This was done using a x-ray Shimadzu 6000 X-ray diffractometer (Figure4-3) with a Cu K_α radiation (λ = 0.154 nm) operated at 40 kV and 30 mA. The XRD patterns were collected at diffraction angles 2θ from 25^o to 80^o in steps of 0.2^o.

Figure 4-3 X-ray Shimadzu 6000 X-ray diffractometer

4.2. X-RAY PHOTOELECTRON SPECTROSCOPY

X-Ray Photoelectron Spectroscopy (XPS) is a surface analysis technique used to provide elemental and chemical information about solid materials. The main components of the XPS instrument are the following: vacuum pumps, sample holder, X-ray source, electrostatic lenses, electrostatic analyzer, channeltron detectors and a computer system as shown in Figure 4-4 [61] .

In each XPS experiment the sample is prepared and inserted in a fast entry chamber which can be evacuated down to 10^{-3} millibar using a rotary pump and a turbomolecular pump. The sample is transferred to a prep-chamber and then transferred to the main chamber where the vacuum reaches about 10^{-9} millibar with the aid of large ion pumps.

In a typical XPS experiment, soft x-rays (1486 eV or 1253.6 eV) irradiate the sample and the subsequent electrons ejected from the inner atomic shells are energy analyzed. The kinetic energy of these electrons, E_{kin} , is equal to the difference between the x-ray energy, hν, and the binding energy, E_B, of the electron according to the following formula

$$E_{kin} = h\nu - E_B$$

Where E_B is the energy difference between the final and the initial states of the electron

$$E_B = E_{ion} - E_{atom}$$

The electrons emitted are collected by electrostatic lenses and inserted into the electrostatic analyzer. The electrostatic analyzer consists of two hemispherical metallic parts. One is concave and the other is convex. The two hemispheres are arranged such that their centers of curvature coincide as shown in Figure 4-5.

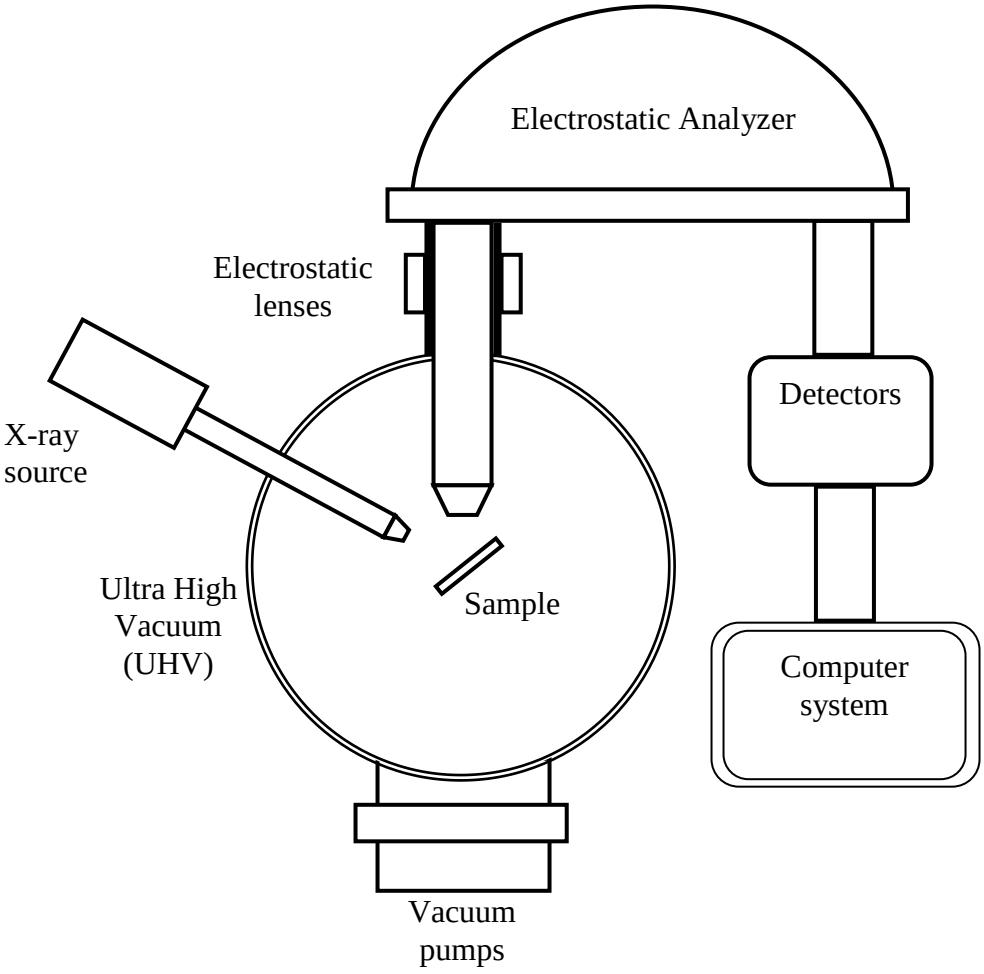

Figure 4-4 Main components of XPS system

A voltage difference is applied between the two hemispheres where the outer one is held at positive voltage and the inner one is grounded such that a radial electrical field is generated. When the electrons pass through electrostatic field analyzer, they will collide with one of the concentric hemispheres or they will just pass through. If the velocity of the electron is high it will collide with the outer hemisphere whereas the electrons will collide with the inner hemisphere if the velocity of electrons is too low. With the right velocity of electron controlling the difference voltage, the electron will pass through the distance between the two hemispheres in order to reach the detector. The electrons detected will be analyzed with a computer system that provides us with a series of photoelectron peaks in a resultant spectrum. The energy of the peaks and the elemental composition of can be determined. The shape of each peak provides about information on the chemical bonding[62- 63].

Figure 4-6 is a photograph of the XPS system, a VG scientific ESCALAB MKII spectrometer, equipped with dual aluminum–magnesium anode using Al Kα radiation (hν = 1486.6 eV), used in our work.

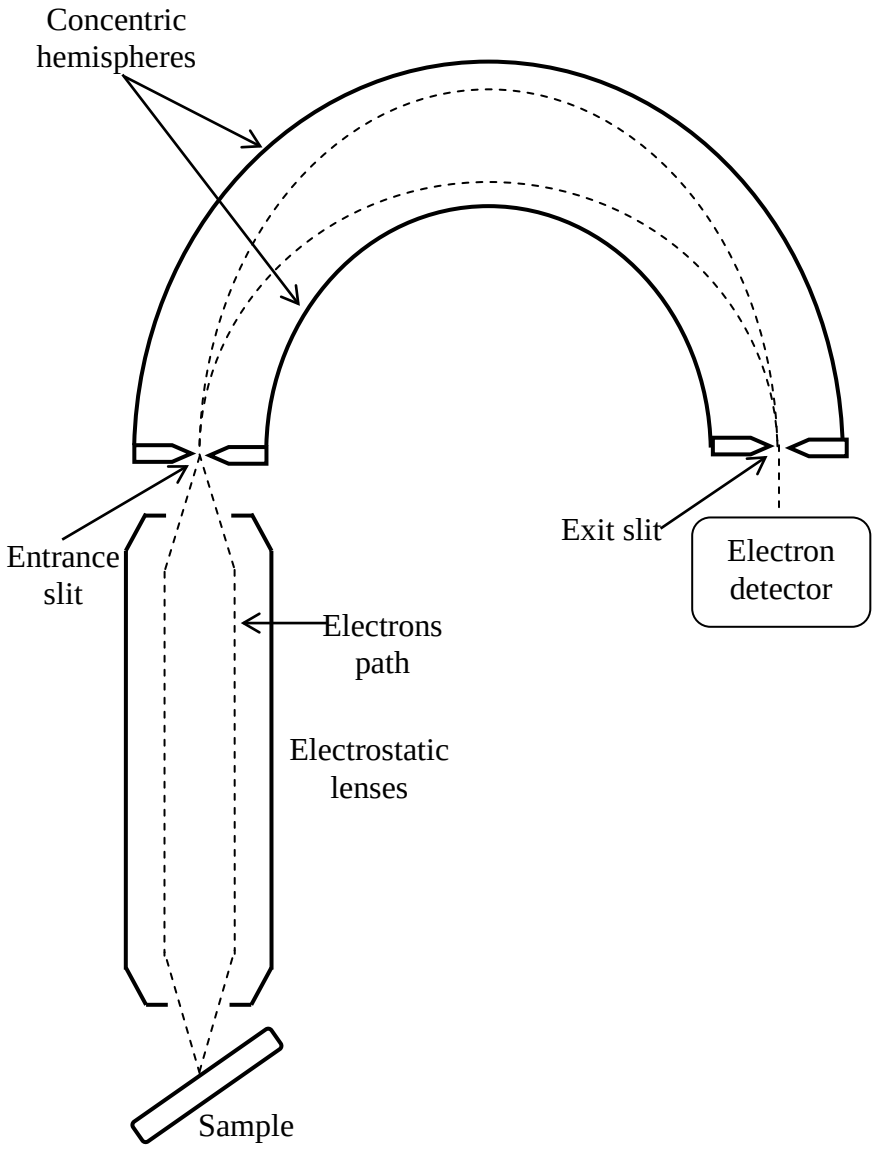

Figure 4-5 Mechanism of X-rays photoelectron spectroscopy

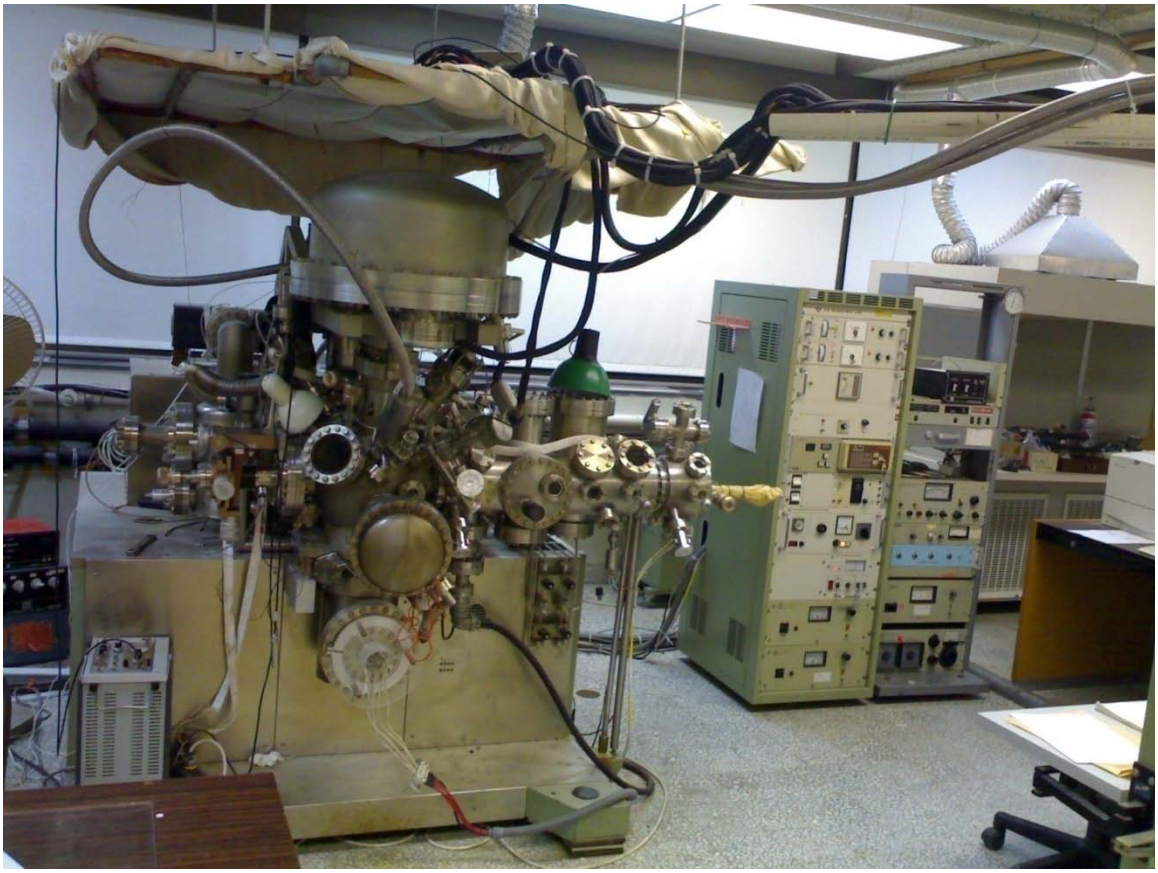

Figure 4-6 X-ray photoelectron microscopy (VG scientific ESCALAB MKII spectrometer).

4.3. FIELD EMISSION SCANNING ELECTRON MICROSCOPY

FESEM term is an acronym for Field Emission Scanning Electron Microscopy. This technique is considered an improvement over Scanning Electron Microscopic (SEM). The electrons scan the sample in zig-zag pattern. FE-SEM has the ability to visualize small objects of 1 nanometer.

The system consists of a source of electrons (a cathode and an anode), electro-magnetic lenses, scanning unit, specimen stage and detectors. The cathode is an extremely thin and sharp needle of tungsten; its diameter is 10^{-7} – 10^{-8} m whereas in standard electron microscopes electrons are produced by heating a tungsten filament. Figure 4-7 shows FESEM structure and working mechanism.

By the high voltage (0.5 to 30 kV) applied on the source of electrons in presence of a high vacuum (10^{-8} torr), a primary electrons beam is generated and accelerated toward electronic lenses. The primary electron beam is produced as a narrow scanning beam and focused by the electro-magnetic lenses that pass through the apertures in the beam column with a sharp before strike the sample. The scan unit deflect the electron beam over the object according to a zig-zag pattern and to correct irregularities in the x and y deflection of the beam.

The electrons beam scans the surface of the sample and interacts with the atoms of the surface. This operation results secondary electrons which are caught by the detector. The detector produces an electronic signal. The signal is amplified and transformed to a

video scan-image that can be seen on a monitor or to a digital image that can be saved and processed further.

The image quality taken with FESEM is better than the image quality taken with the scanning electron microscopy (SEM) due to the electron beam in FESEM is much smaller than the electron beam in SEM [64- 65].

In our work, the morphology of pure and doped ZnO samples was investigated by Tescan model Lyra-3, FESEM.

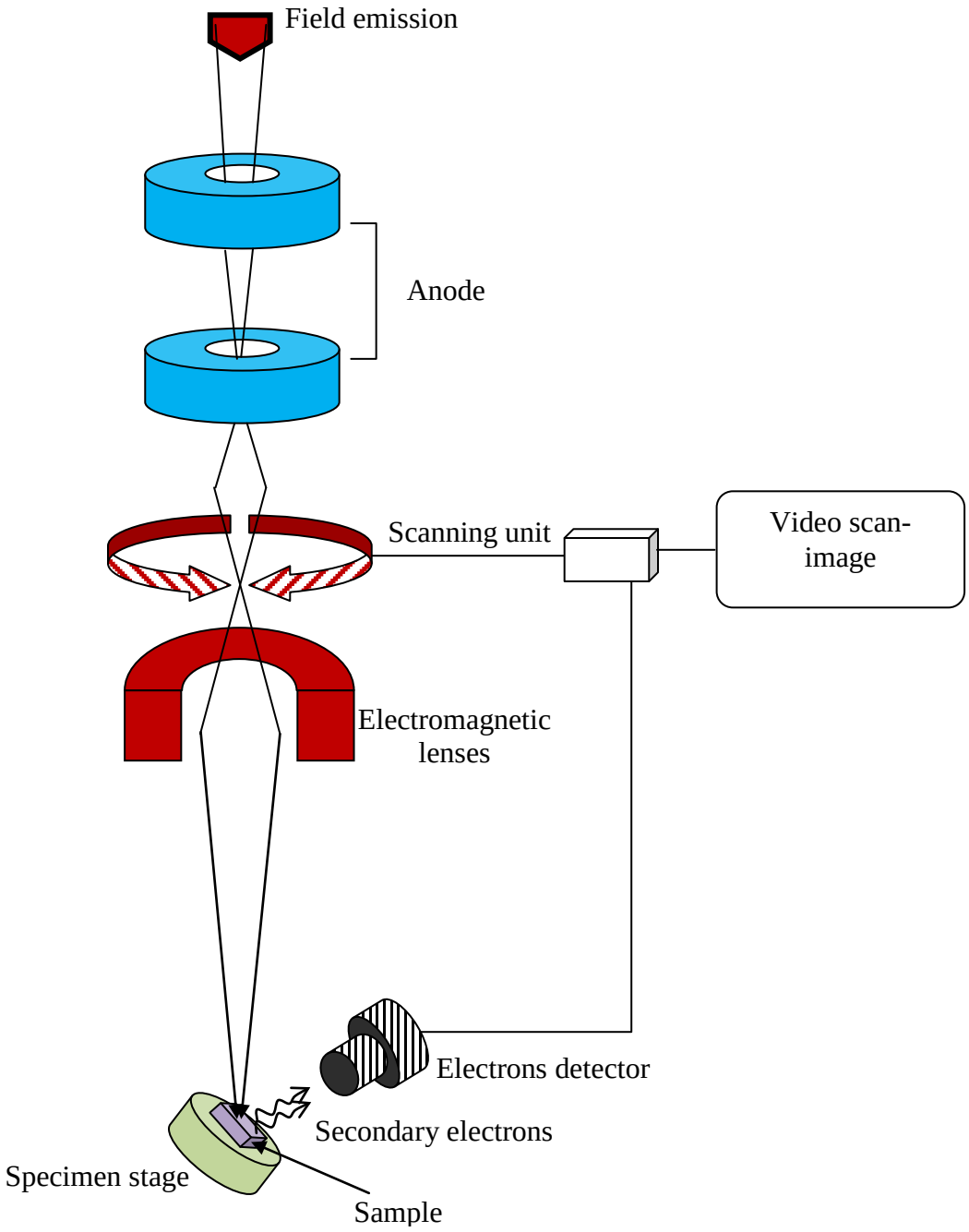

Figure 4-7 Components of FESEM

4.4. UV-VISIBLE DIFFUSE REFLECTANCE SPECROSCOPY

UV – visible diffuse reflectance spectroscopy is a technique used to measure the ability of the material reflectance of light when the material is excited by the visible and adjacent Ultraviolet light.

In opaque materials such as solids, the absorbance coefficient of light is given by Kubelka – Munk function $F(R_\infty)$

$$\frac{K}{S} = \frac{(1 - R_\infty)^2}{2R_\infty} \equiv F(R_\infty)$$

where *K* Kubelka-Munk absorption coefficient for solid materials, and

$R_\infty = \left(\frac{R_{Sample}}{R_{Standard}}\right)$ and S scattering coefficient of the sample[66].

The direct band gap energy E_g is estimated with Tauc's equation

$$(\alpha E)^2 = C_1(E - E_g)$$

where α absorption coefficient of the sample, E photon energy and C_1 constant.

In case of a solid material, when the diffuse reflectance of the material is perfectly carried out, K equals to 2α and S becomes constant for all wavelengths so Tauc's

equation is reformulate to the new form

$$[K\,E]^2 = C_2(E - E_g)$$

By representing the correlation between $[K\,E]^2$ on y- axis versus E on x-axis, the intersection point of extrapolating the straight line on x- axis, at $[K\,E]^2 = 0$, represents E_g[67].

Figure 4-8 exhibits the design of UV-visible spectroscopy used in measurement of diffuse reflectance for solid materials. The light is passed through the exit slit monochromater and then focused on the sample by the lens and mirror. The light is diffusely reflected by the sample and then collected with the integrating sphere. The reflected light was obtained and recorded as data via the photomultiplier.

The UV-visible spectrophotometer (Labsphere-Evolution 600) in Figure 4-9 was used for determining the band gap energy. UV-visible spectrophotometer is adjusted to obtain a reflectance spectrum in the range of UV (200–400 nm) and visible (400–600 nm) regions.

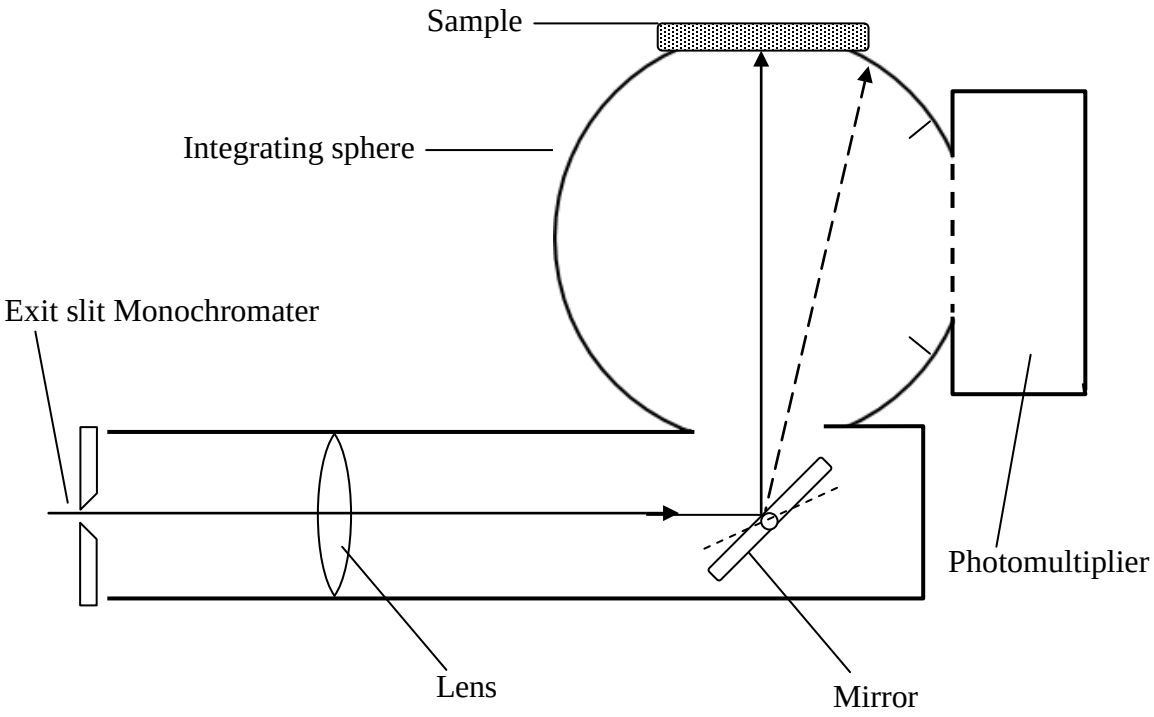

Figure 4-8 UV-visible spectroscopy for analyzing the diffuse reflectance of solid materials.

Figure 4-9 UV-visible spectrophotometer (Labsphere-Evolution 600)

CHAPTER 5

RESULTS AND DISCUSSION

5.1. PURE ZNO CHARACTERIZATION

5.1.1. XRD results

5.1.1.1. Crystalline structure

Pure ZnO has been prepared with four concentrations 1, 2, 3, and 4% of zinc acetate as precursor material by microwave assisted polyol method at 180 °C and 200 °C.

Obtained ZnO Nanopowders were characterized by X-ray powder diffraction (XRD) in the range of 25–80° with a scanning step of 0.02°. Figure 5-1 shows XRD diffraction patterns for a sample of pure ZnO. It can be seen that all peaks indicate a single hexagonal phase of ZnO. No other peaks for any phase can be found. As it was observed that the sample characterized does not contain contamination or impurities. The grain size has been estimated from Scherer's equation

$$g = \frac{0.9\ \lambda}{\beta \cos\theta}$$

where, g is the diameter of the grain size, λ is the wavelength of x-ray radiation source, $\beta \equiv \sqrt{\beta_m^2 - \beta_s^2}$ where β_m is the measured peak width and β_s is the instrumental peak width.

The grain size has been determined in the range from 8 to 13 nm and from12 to 17 nm at 180 °C and 200 °C for 2% of precursor materials, respectively.

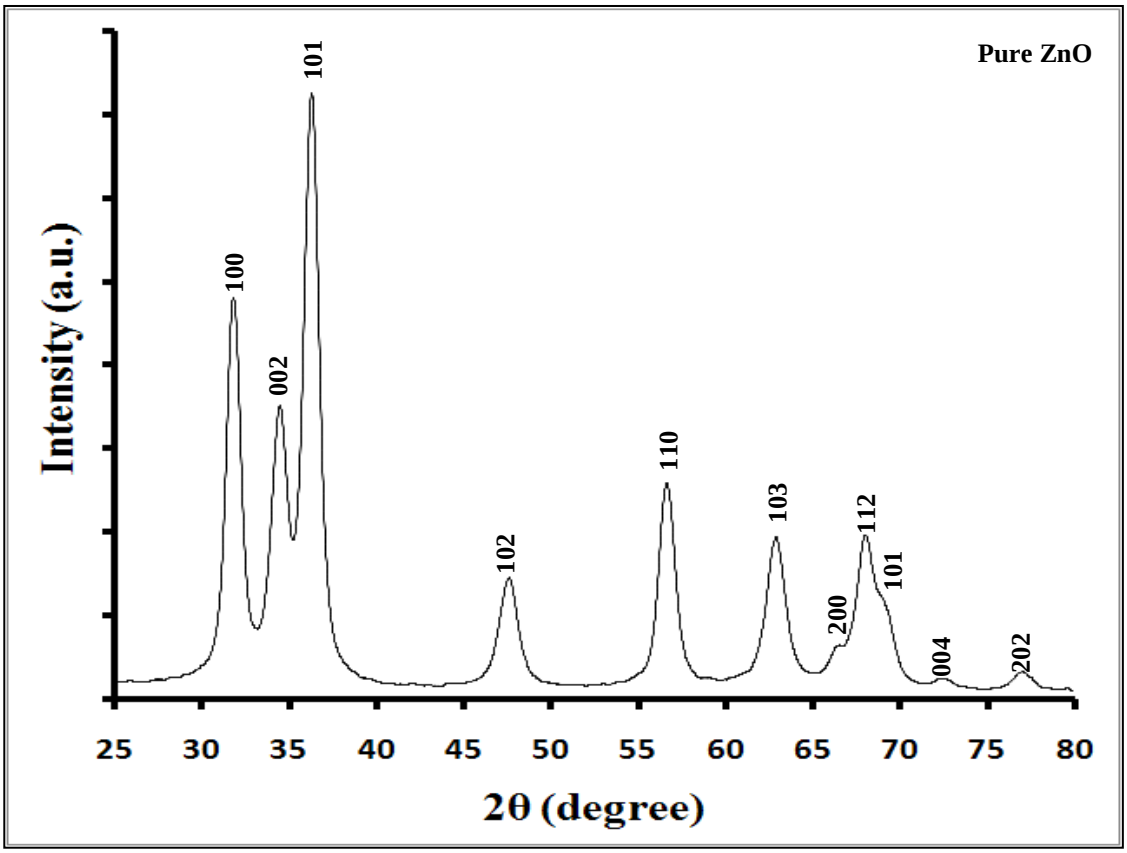

Figure 5-1 Hexagonal phase of pure ZnO synthesized by microwave assisted polyol method at 180 °C for 2% of precursor materials

5.1.1.2. Effect of precursor material (zinc acetate) concentration on the particle size.

Concentration effects of the precursor material (zinc acetate) on the grain size were studied by XRD. Values of the grain size have been estimated for the diffraction intensity of (100) peak by Scherer's equation.

Figure 5-2 depicts a relation between concentrations of the precursor material (zinc acetate) and the grain size. We observe that the grain size increases with increasing concentrations of the precursor material. As we found that the grain size is larger at synthesis temperature of 200 °C.

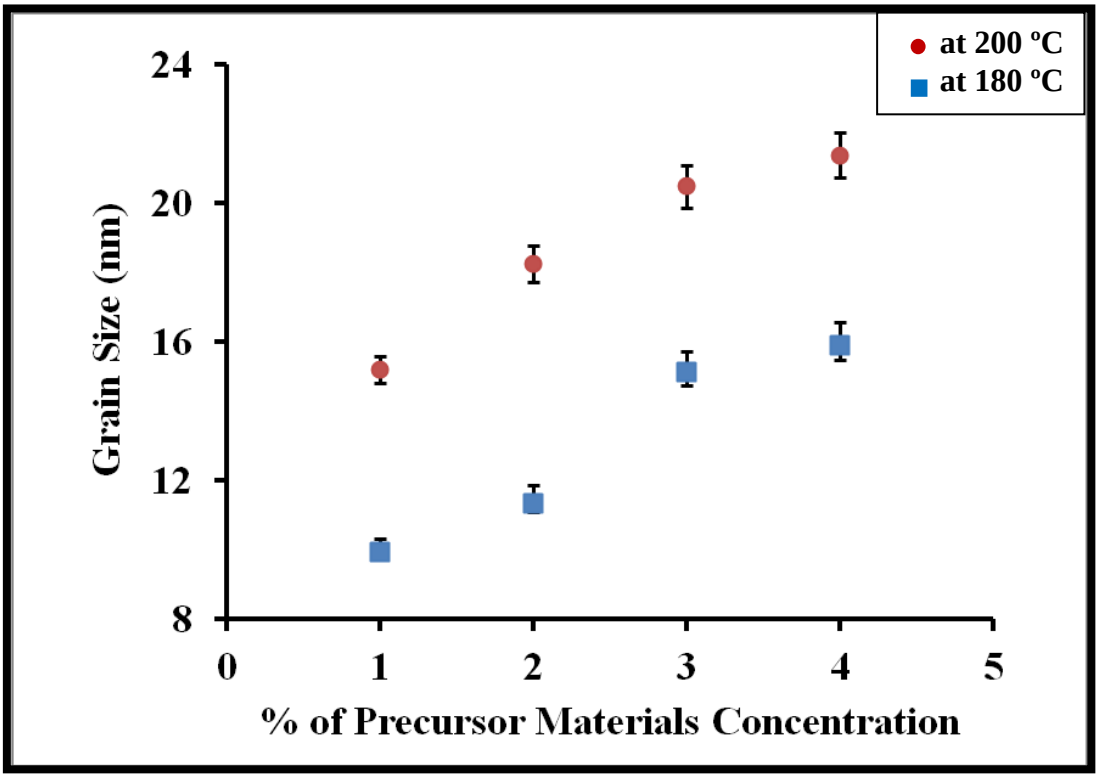

Figure 5-2 Correlation between the grain size and concentration of the precursor material synthesized by microwave assisted polyol method at 180 °C and 200 °C

5.1.2. XPS results

Figure 5-3 exhibits the XPS survey spectrum (0 – 1200 eV) of pure ZnO synthesized at 180 °C. All elements that showed within the spectrum were ascribed to Zn, O and C according to XPS handbook[68].

The characteristic binding energy peaks of Zn were found at photoelectron lines $2p_{3/2}$ and $2p_{1/2}$. The binding energy peak of O_2 was at photoelectron line O1s. The $Zn2p_{3/2}$ line was resolved, by Gaussian-Lorentz fitting, into three binding energy peaks located at the 1019.66, 1021.09 and 1023.04 eV as shown in Figure 5-4. The O1s peak was resolved into three binding energies peaks located at 529.35, 531.34 and 533.22eV as shown in Figure 5-5.

The middle peak (1021.09eV) of Zn2p3/2 is attributed to Zn^{+2} in ZnO lattice whereas the others binding energies peaks are of unknown components for Zn within the sample [69-70].

The low binding energy of O1s is related to O^{-2} ions on oxygen deficient regions whereas the high binding energy was coming from loosely bound oxygen existing on the surface of the sample such as OH bond. The middle peak represents the oxygen in ZnO lattice. Carbon at C1s peak (284.5 eV) was utilized as reference to define the correct peak position [69–71].

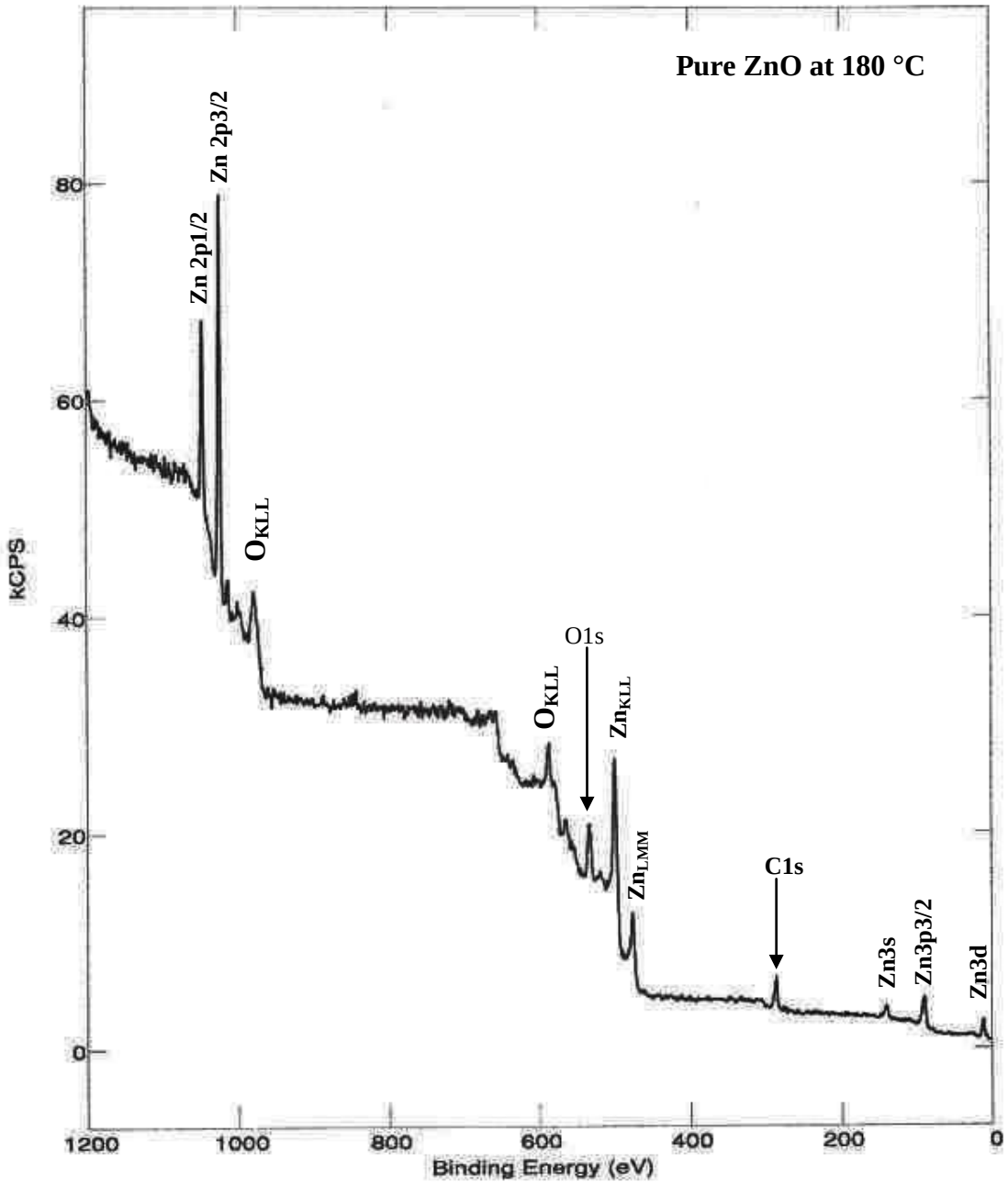

Figure 5-3 XPS spectrum of pure ZnO synthesized at 180 °C by microwave assisted polyol method, showing binding energies peaks corresponding to Zn 2p, O 1s and C1s.

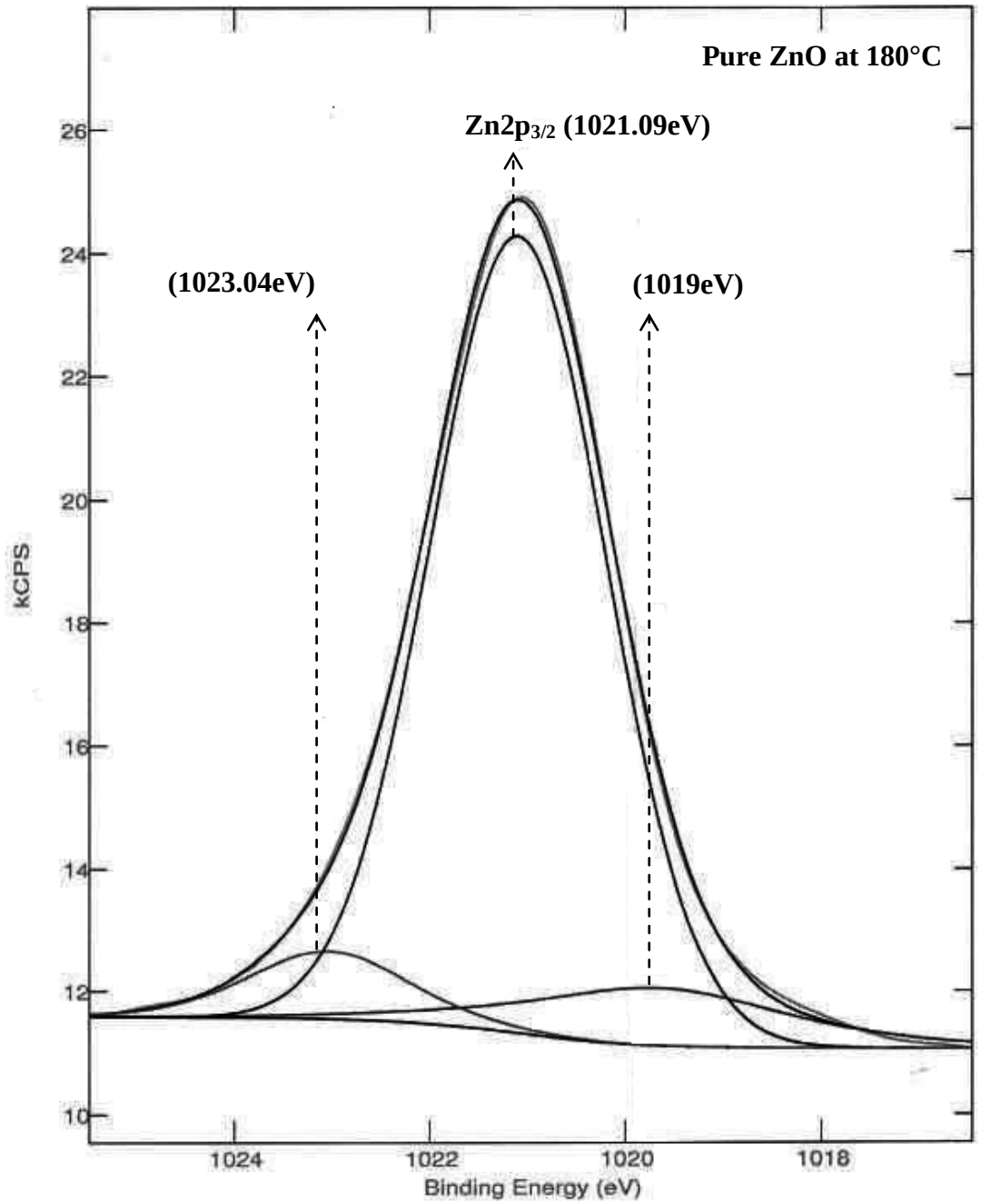

Figure 5-4 Resolving the binding energy peak of Zn $2p_{3/2}$ into three peaks for pure ZnO synthesized at 180 °C

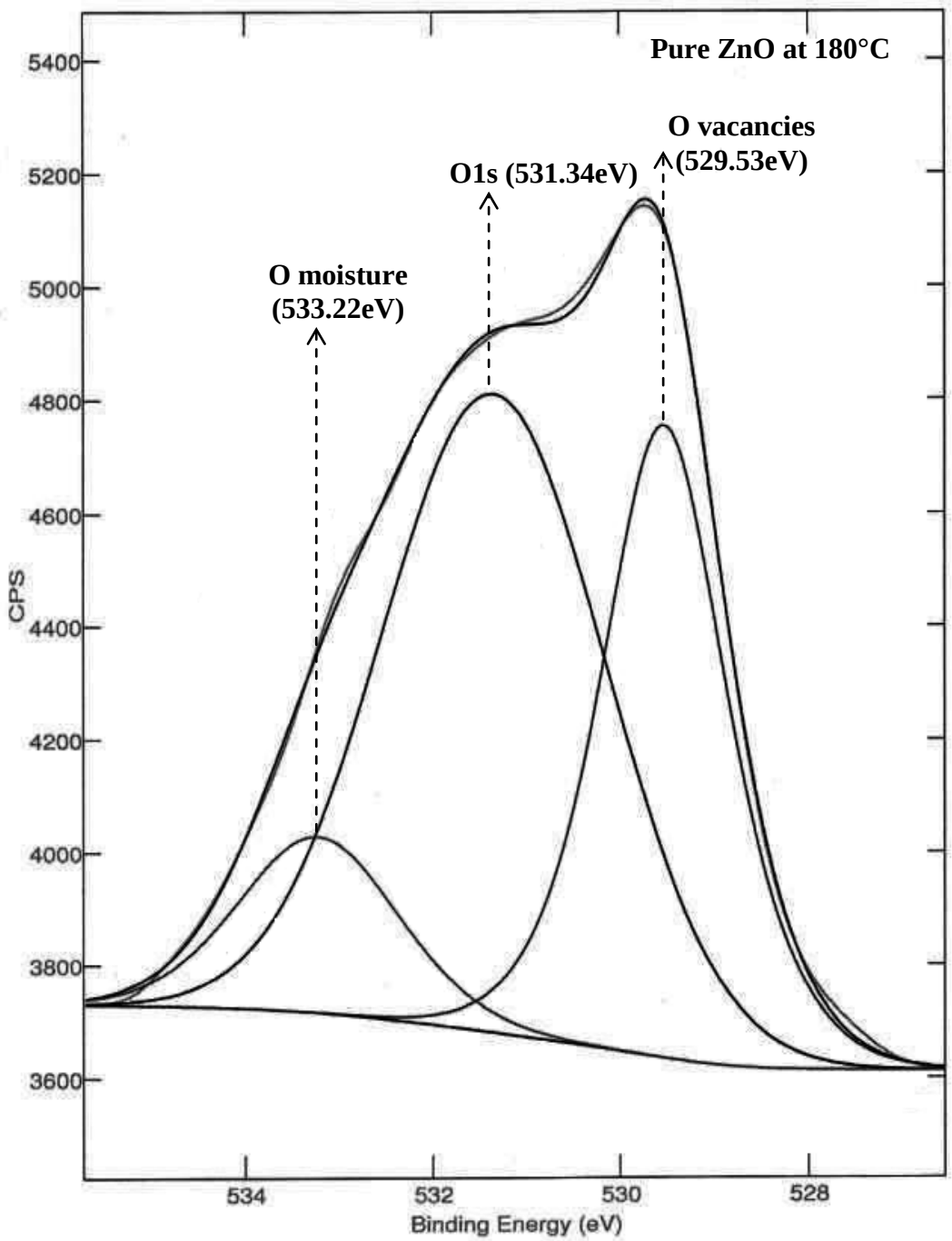

Figure 5-5 Resolving the binding energy peak of O1s into three peaks for pure ZnO synthesized at 180 °C.

5.1.3. FESEM results

Figures 5-6 and 5-7 show FESEM images of two pure samples of ZnO synthesized by microwave assisted polyol method at 180 °C and 200 °C. Images a and b have representative low magnification images while image c was a representative high magnification image. All images demonstrate that nanoparticles strongly agglomerated to large spherical particles.

Synthesis temperature has a distinct role in forming agglomeration of nanoparticles as can be seen in Figures 5-6 and 5-7. Figure 5-6 shows images of separated large spherical particles consisting of similar grains size with a uniform agglomeration for a sample synthesized at 180 °C whereas Figure 5-7 shows sphere-like particles with irregular shapes for a sample synthesized at 200 °C. This change in shapes can be attributed to increasing synthesis temperature [72].

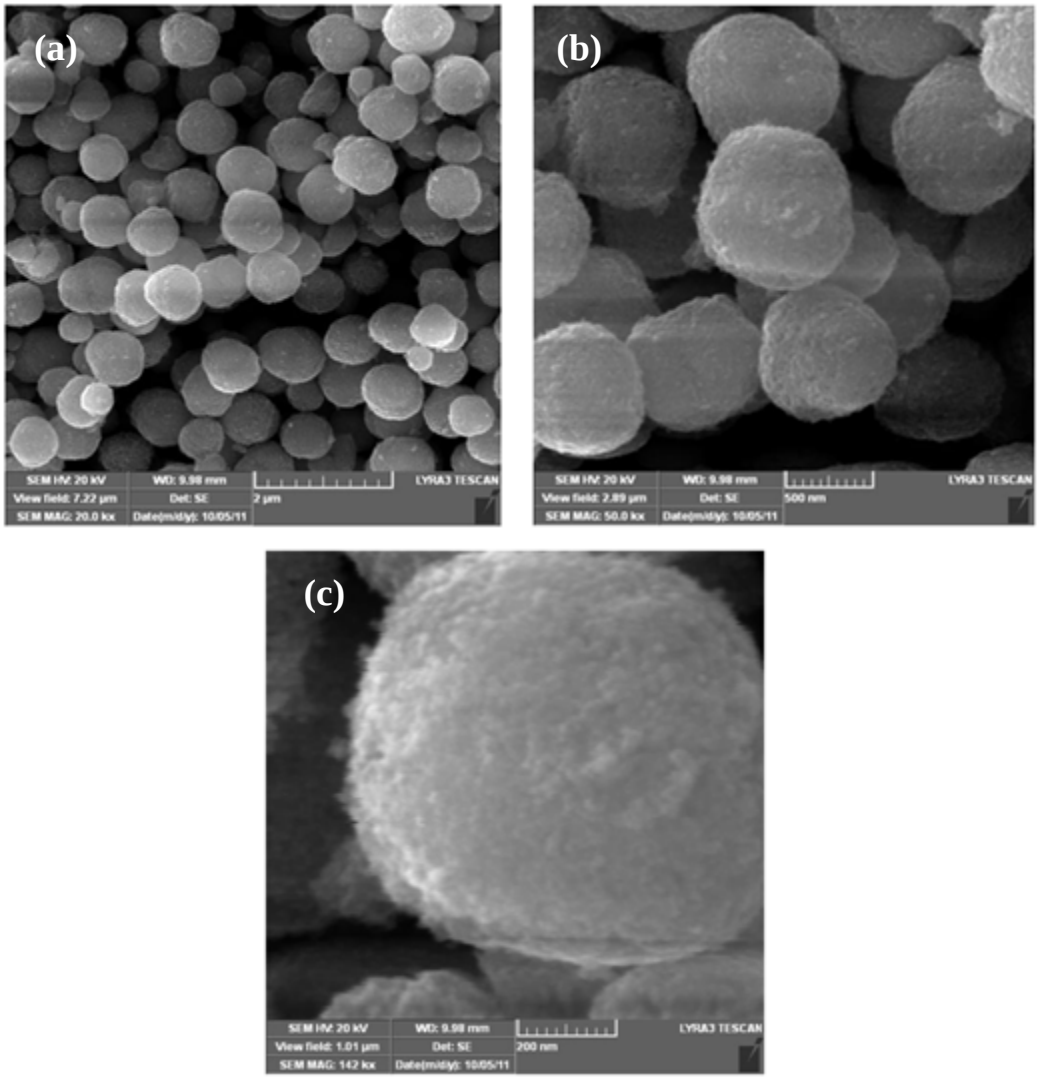

Figure 5-6 Morphology of a pure sample of ZnO synthesized at a temperature of 180 °C via microwave assisted polyol method.

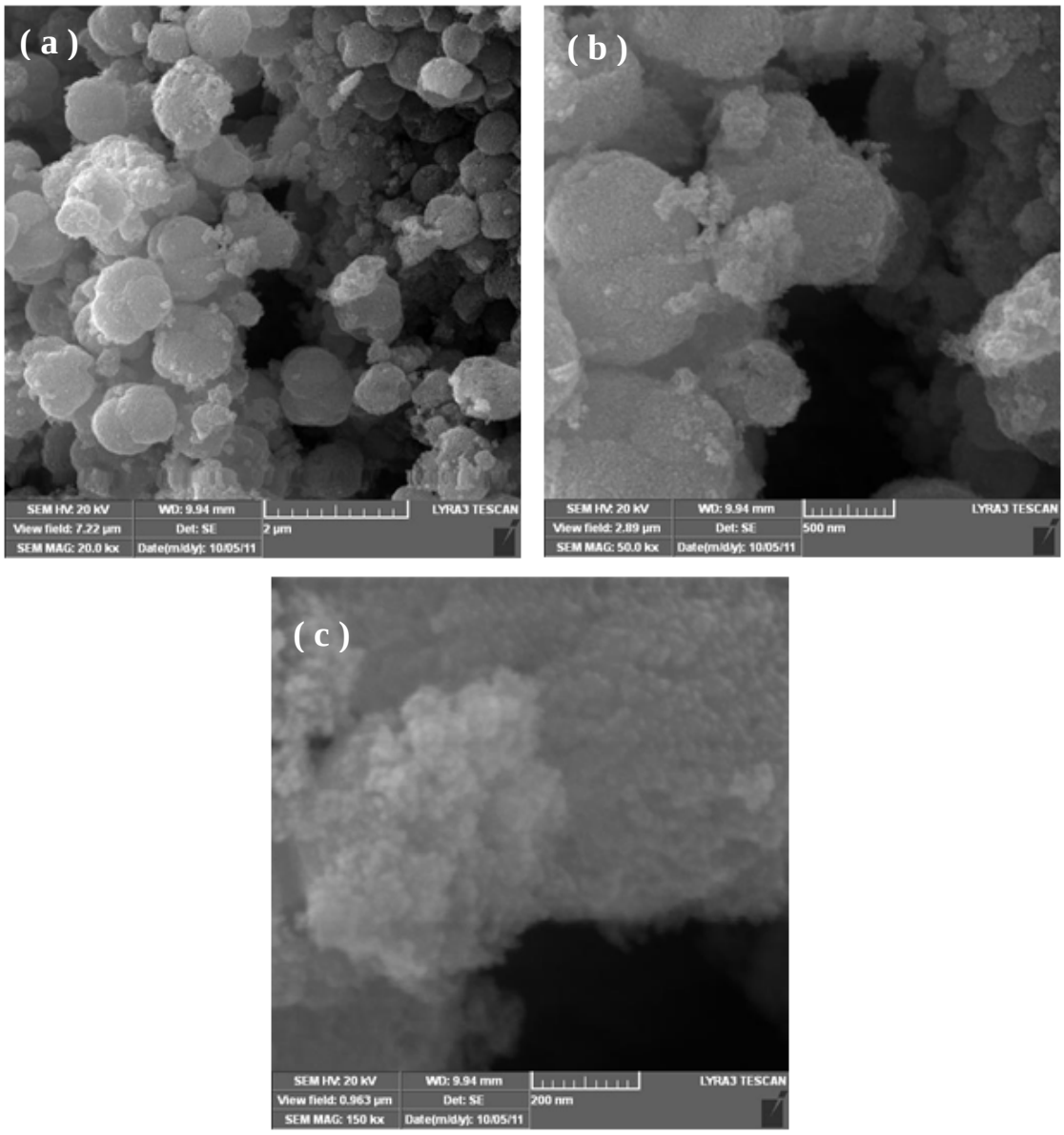

Figure 5-7 Morphology of a pure sample of ZnO synthesized at a temperature of 200 °C via microwave assisted polyol method.

5.1.4. EDS results

Figure 5-8 shows the energy-dispersive spectroscopy (EDS) results of the pure samples synthesized by microwave assisted polyol method at two temperatures 180 °C and 200 °C, respectively. The chemical composition of samples indicates only two components; Zn and O. The spectra emphasize clearly the absence of any impurities in the samples but C peak coming from the tape was used to fix the sample

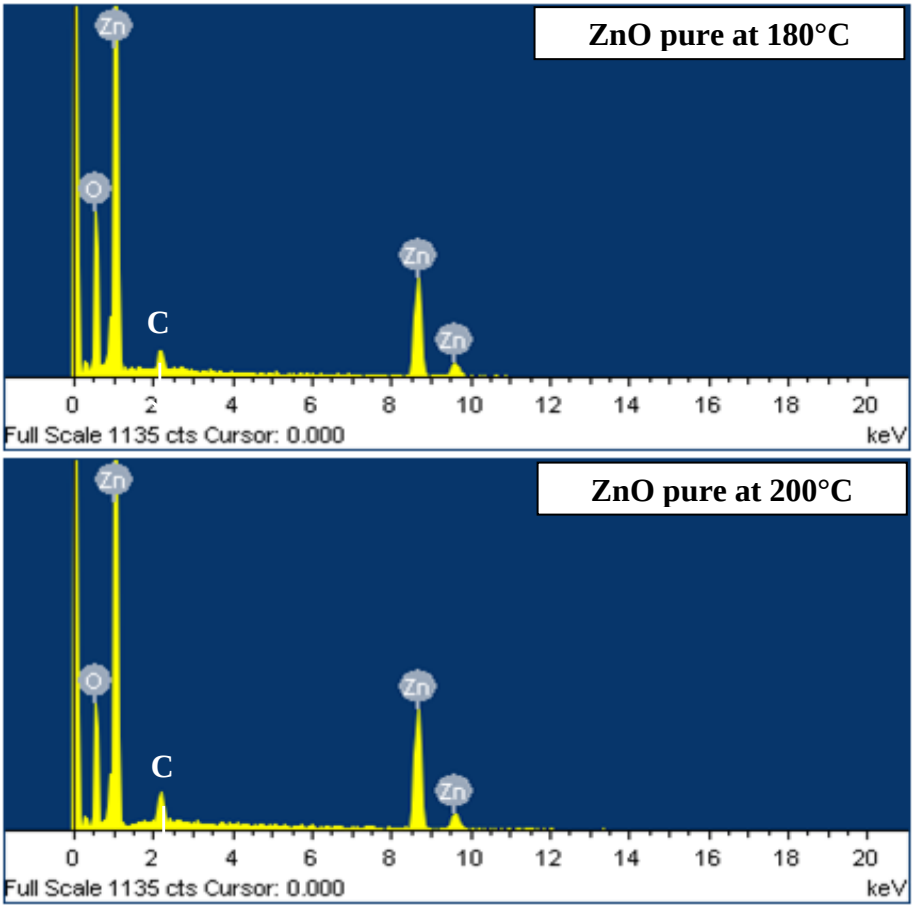

Figure 5-8 Spectra and table showing the chemical purity and components ratios of pure ZnO synthesized via microwave assisted polyol method at180°C and 200 °C.

5.1.5. UV-visible diffuse reflectance spectroscopy results:

Figure 5-9 depicts a correlation between $(K\ E)^2$ and $h\nu$ (photon energy) for one sample of pure ZnO. Using Tauc's equation [67]

$$[K\ E]^2 = C_2(E - E_g)$$

where K Kubelka Munk absorption coefficient, C_2 is constant, $E = h\nu$ is Photon energy, $E_g$is the band gap energy.

We determined the band gap energy for the pure sample by extrapolating of the straight line to $h\nu$ axis at $(K\ E)^2 = 0$ where intersection point of the straight line on $h\nu$ axis represents the band gap energy(E_g). The value of band gap energy of pure ZnO was 3.29 eV at 180 °C.

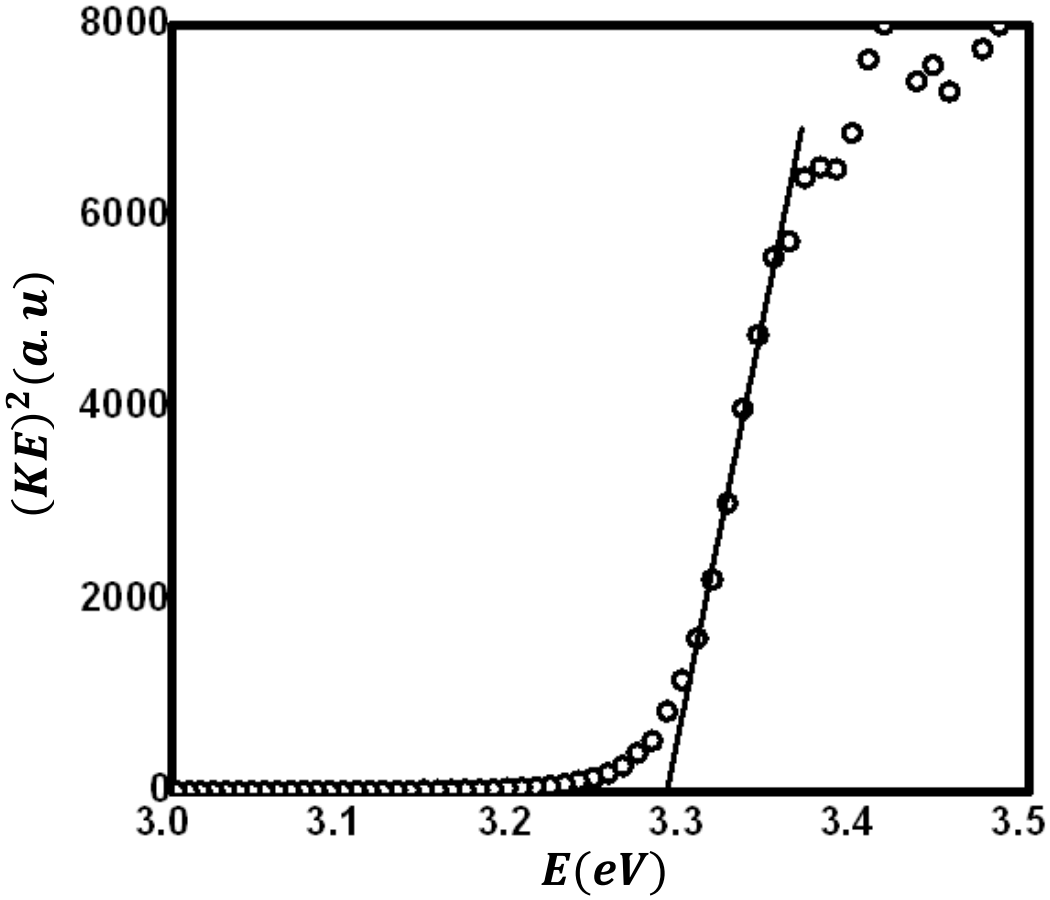

Figure 5-9 The correlation between $(K E)^2$ and E (photon energy) for samples of pure ZnO synthesized by microwave assisted polyol method at 180 ^{0}C for determining the band gap (Eg).

5.2. CU-DOPED ZNO CHARACTERIZATION

5.2.1. XRD results

5.2.1.1. Crystalline structure of Cu-doped ZnO

Figures 5-10, 5-11, 5-12 and 5-13 show the spectra of x-ray diffraction patterns for pure and doped ZnO ($Zn_{1-x}Cu_xO$ (x = 0.0, 0.02, 0.04, 0.06, 0.08, 0.10, 0.12 and 0.14)) at temperature (a) 180 °C and (b) 200 °C. The XRD results revealed that diffraction peaks of all samples are similar to the hexagonal structure of ZnO. In addition, other peaks were observed within the hexagonal phase of ZnO in the doped samples. One peak of Al is coming from the sample holder. The other peaks which were found at diffraction angles 42.54° and 61.66° indicatedCu_2O structure. It can be seen that their intensity increases with the increase of doping concentration. Cu_2O phase formed out of the lattice crystal of ZnO since Cu^{+1} radius (0.096 nm) of Cu_2O is larger than Zn^{+2} radius (0.074 nm) of ZnO. In other hand, Cu^{+2} of CuO can replaced Zn^{+2} in the crystal since Cu^{+2} radius (0.072 nm) since its ionic radius is very close to the Zn^{+2} radius (0.074 nm)[73]. No CuO phase showed up in the XRD spectrum for all doping concentrations. This is due to the random substitution of Zn^{+2} by Cu^{+2} and/or the existence of Cu atoms as interstitials in the ZnO lattice. However, it is possible that CuO phase can be formed when the concentration of Cu exceeds the solubility limit of Cu^{+2} in ZnO (10-16%)[74].

It can be seen also that, no peaks had a clear shift in the doped samples compared to pure samples. This phenomenon was also observed and attributed to the similarity of Cu and Zn radii[75].

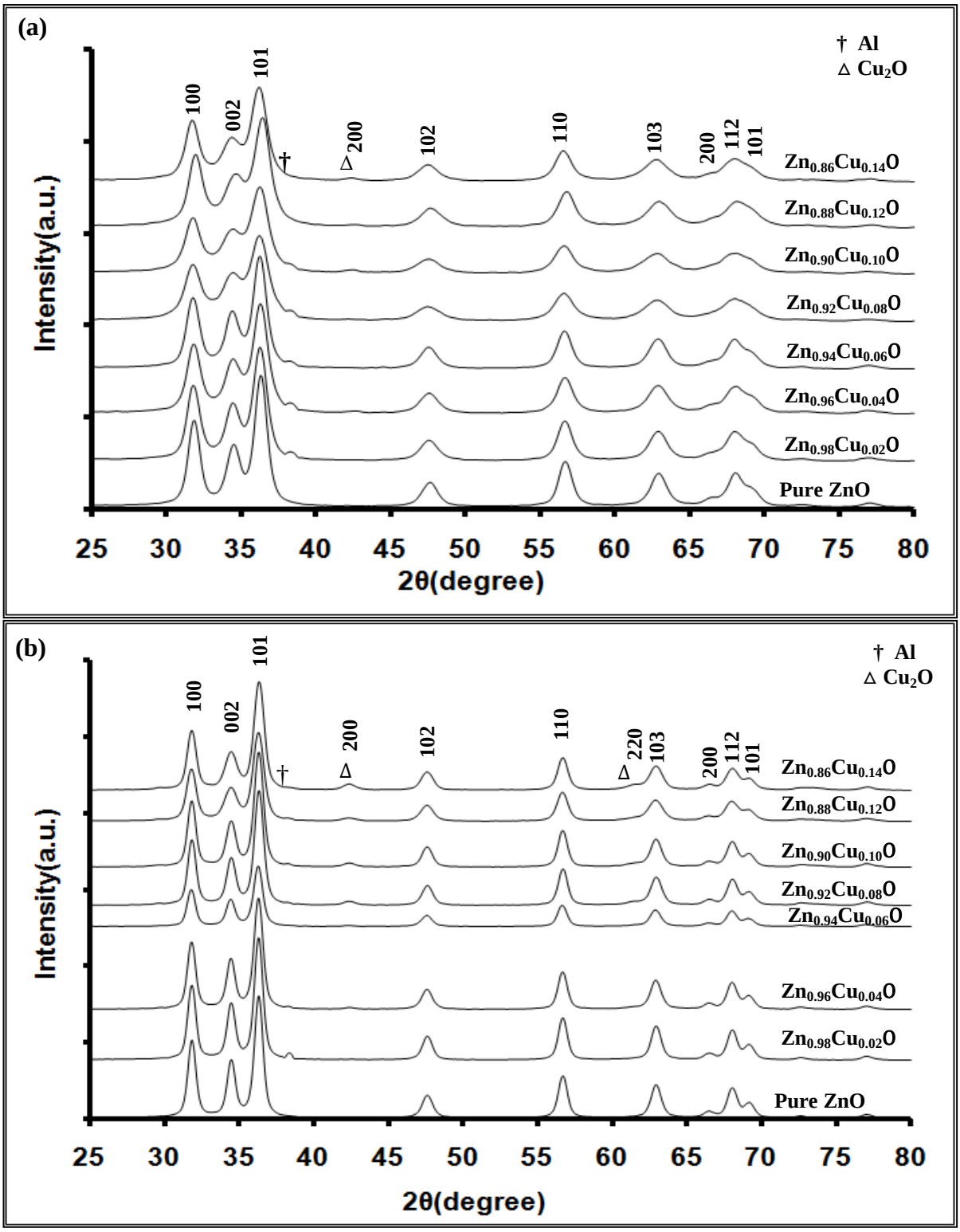

Figure 5-10 XRD diffraction patterns for $Zn_{1-x}Cu_xO$ synthesized by Microwave assisted polyol method at temperature of (a)180 °C and (b)200 °C for 1% precursor materials.

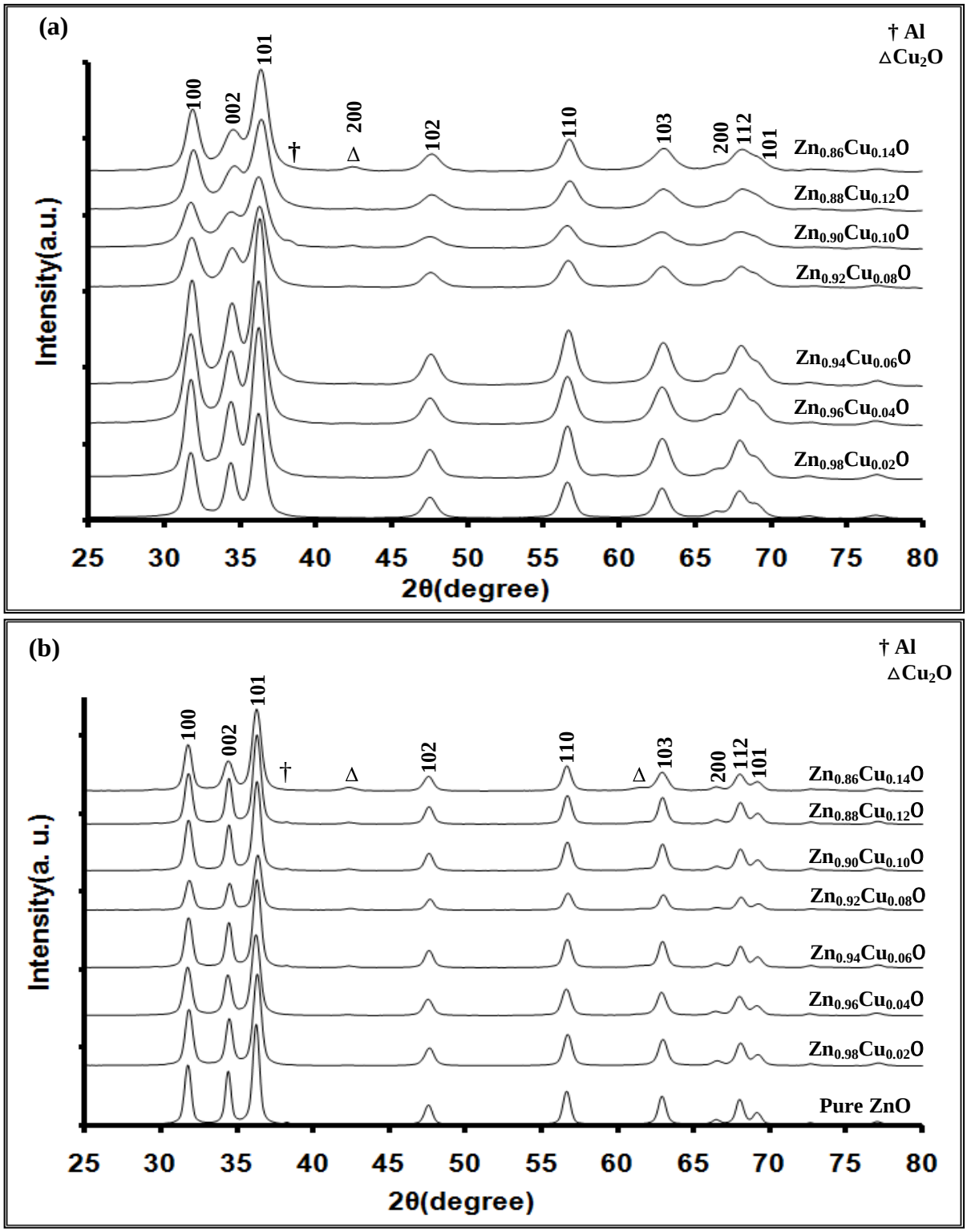

Figure 5-11 XRD diffraction patterns for $Zn_{1-x}Cu_xO$ synthesized by Microwave assisted polyol method at temperature of (a)180 °C and (b)200 °C for 2% precursor materials.

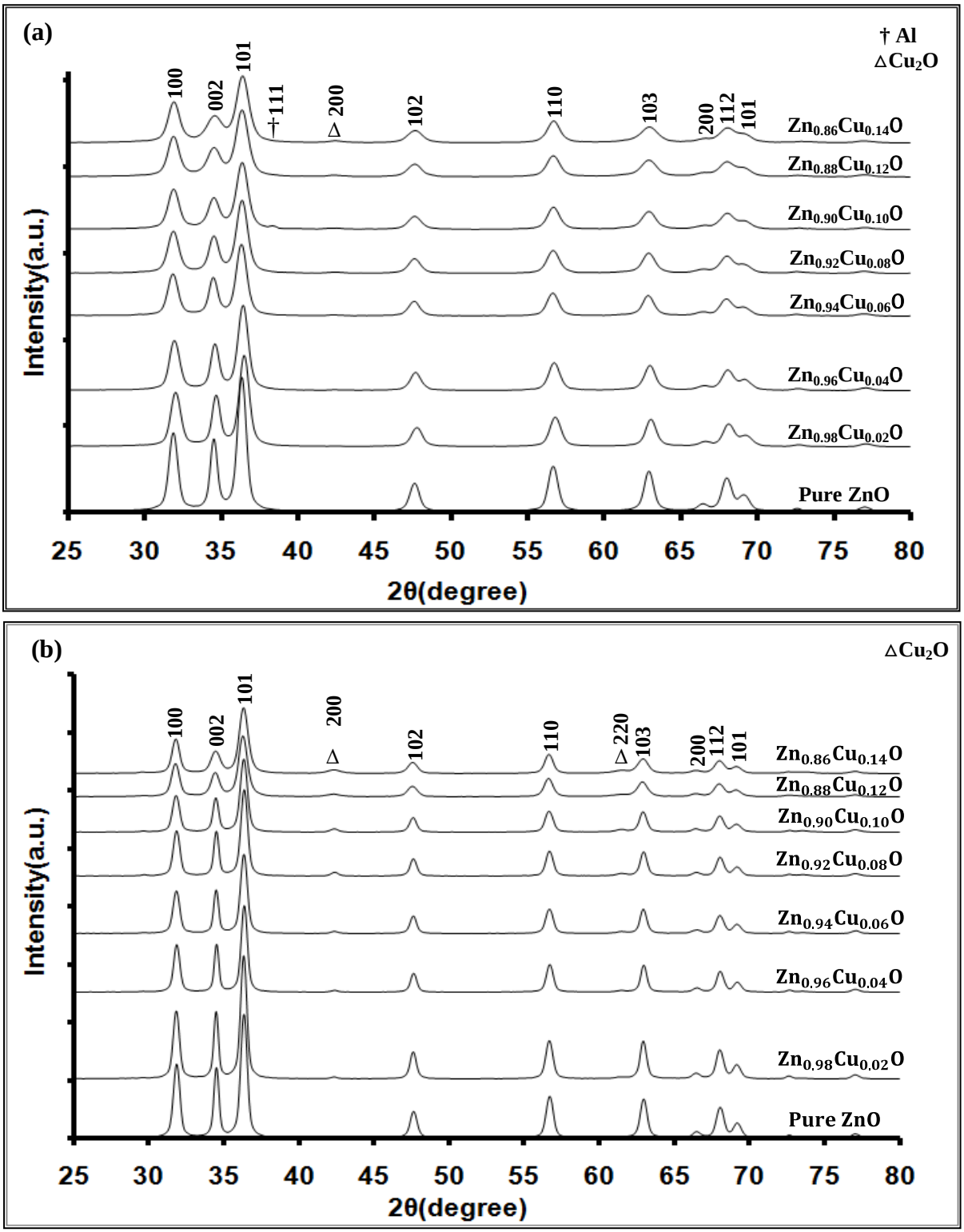

Figure 5-12 XRD diffraction patterns for $Zn_{1-x}Cu_xO$ synthesized by Microwave assisted polyol method at temperature of (a)180 °C and (b)200 °C for 3% precursor materials.

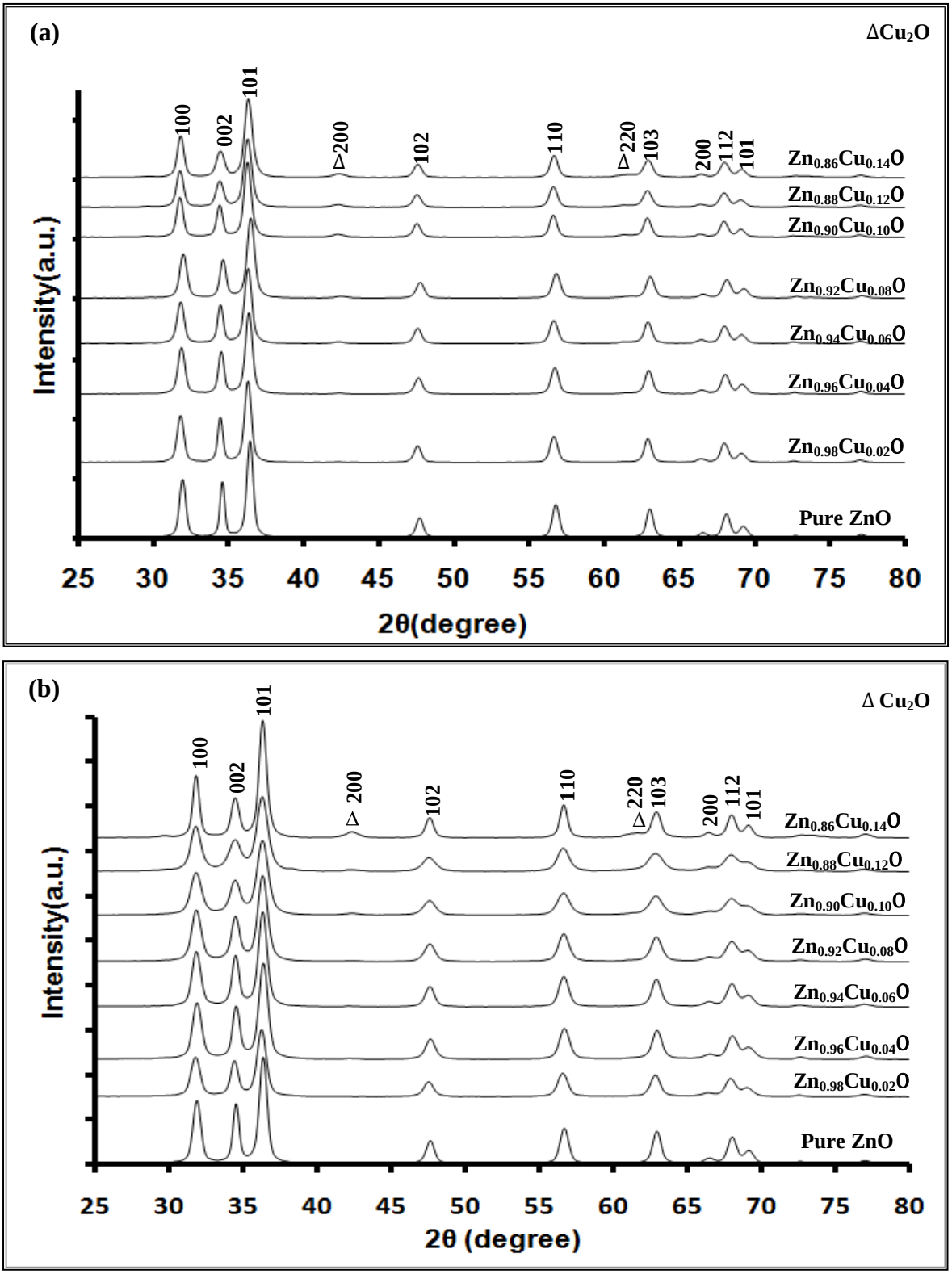

Figure 5-13 XRD diffraction patterns for $Zn_{1-x}Cu_xO$ synthesized by Microwave assisted polyol method at temperature of (a)180 °C and (b)200 °C for 4% precursor materials.

5.2.1.2. Doping Effect on the lattice parameters of ZnO structure

Effect doping on the lattice parameters of ZnO was studied for pure and doped samples fabricated with microwave assisted polyol method at two different temperature 180 °C and 200 °C. The structure of ZnO is hexagonal with lattice parameters a, b and c. The lattice parameters a=b and c of ZnO have been determined through the two highest peaks of diffraction angles at indexes (100) and (002) respectively using the two following formulas

$$a = b = \frac{0.9\ \lambda}{\sqrt{3}\ \sin\alpha} \quad \text{and} \quad c = \frac{0.9\ \lambda}{\sin\gamma}$$

Values of the lattice parameters obtained for all synthesized sample were recorded in Table 5-1 and Table 5-2. They clearly show no changes in the lattice parameters in all investigated samples. This is due to the similarity of Cu and Zn radii[75]

Table 5-1 Data of lattice parameters a = b and c of all samples of undoped and doped ZnO at 180 °C

% of Cu Concentration	1% of precursor materials		2% of precursor materials		3% of precursor materials		4% of precursor materials	
	a(Å)	*c(Å)*	*a(Å)*	*c(Å)*	*a(Å)*	*c(Å)*	*a(Å)*	*c(Å)*
0	3.24	5.19	3.25	5.21	3.24	5.20	3.24	5.19
2	3.24	5.21	3.25	5.20	3.23	5.18	3.25	5.21
4	3.24	5.20	3.25	5.20	3.24	5.19	3.24	5.19
6	3.25	5.21	3.24	5.19	3.25	5.21	3.24	5.20
8	3.25	5.21	3.24	5.20	3.24	5.20	3.24	5.20
10	3.25	5.20	3.25	5.22	3.25	5.22	3.24	5.20
12	3.23	5.17	3.25	5.21	3.24	5.19	3.25	5.20
14	3.25	5.22	3.23	5.19	3.24	5.19	3.25	5.20

Table 5-2 Data of lattice parameters a = b and c of all samples of undoped and doped ZnO at 200 °C

% of Cu Concentration	1% of precursor materials		2% of precursor materials		3% of precursor materials		4% of precursor materials	
	a(Å)	*c(Å)*	*a(Å)*	*c(Å)*	*a(Å)*	*c(Å)*	*a(Å)*	*c(Å)*
0	3.24	5.20	3.25	5.20	3.24	5.19	3.23	5.18
2	3.24	5.20	3.24	5.19	3.24	5.20	3.25	5.20
4	3.25	5.20	3.25	5.21	3.2	5.19	3.24	5.19
6	3.25	5.21	3.24	5.20	3.24	5.20	3.24	5.20
8	3.24	5.20	3.24	5.19	3.24	5.20	3.23	5.18
10	3.24	5.20	3.24	5.19	3.24	5.20	3.25	5.21
12	3.25	5.20	3.25	5.21	3.25	5.21	3.25	5.21
14	3.24	5.20	3.25	5.20	3.25	5.20	3.24	5.20

5.2.1.3. Estimating grain size of pure and doped ZnO

Figures5-14 and 5-15 show the effect doping concentration on the grain size of Cu doped ZnO samples that are synthesized at180 °C and 200 °C. The grain size has been estimated by Sherrer's equation[76]:

$$g = \frac{0.9\ \lambda}{\beta\cos\theta}$$

where, g is the diameter of the grain size, λ is the wavelength of x-ray radiation source, $\beta \equiv \sqrt{\beta_m^2 - \beta_s^2}$ where β_m is the measured peak width and β_s is the instrumental peak width.

The grain size of nanoparticles doped with Cu decreases with increasing Cu concentration as recorded in Table 5-3 and shown Figures 5-14 and 5-15. This can be attributed to the inhibition of grain growth due to the incorporating CuO into ZnO clusters[77].

Table 5-3 Data showing the correlation of Cu concentration and the grain size of synthesized samples by microwave assisted polyol method at 180 ºC and 200 ºC

Grain size (nm)								
% of Cu Concentration	1 % of precursor materials		2 % of precursor materials		3 % of precursor materials		4 % of precursor materials	
	180ºC	*200ºC*	*180ºC*	*200ºC*	*180ºC*	*200ºC*	*180ºC*	*200ºC*
0	10	16	12	21	16	21	16	22
2	9	16	10	18	14	23	15	21
4	9	15	10	16	13	23	15	20
6	10	15	10	18	13	20	15	19
8	7	14	9	18	12	20	14	19
10	7	14	9	16	12	19	12	19
12	8	12	9	15	11	15	12	17
14	8	13	9	15	11	15	11	18

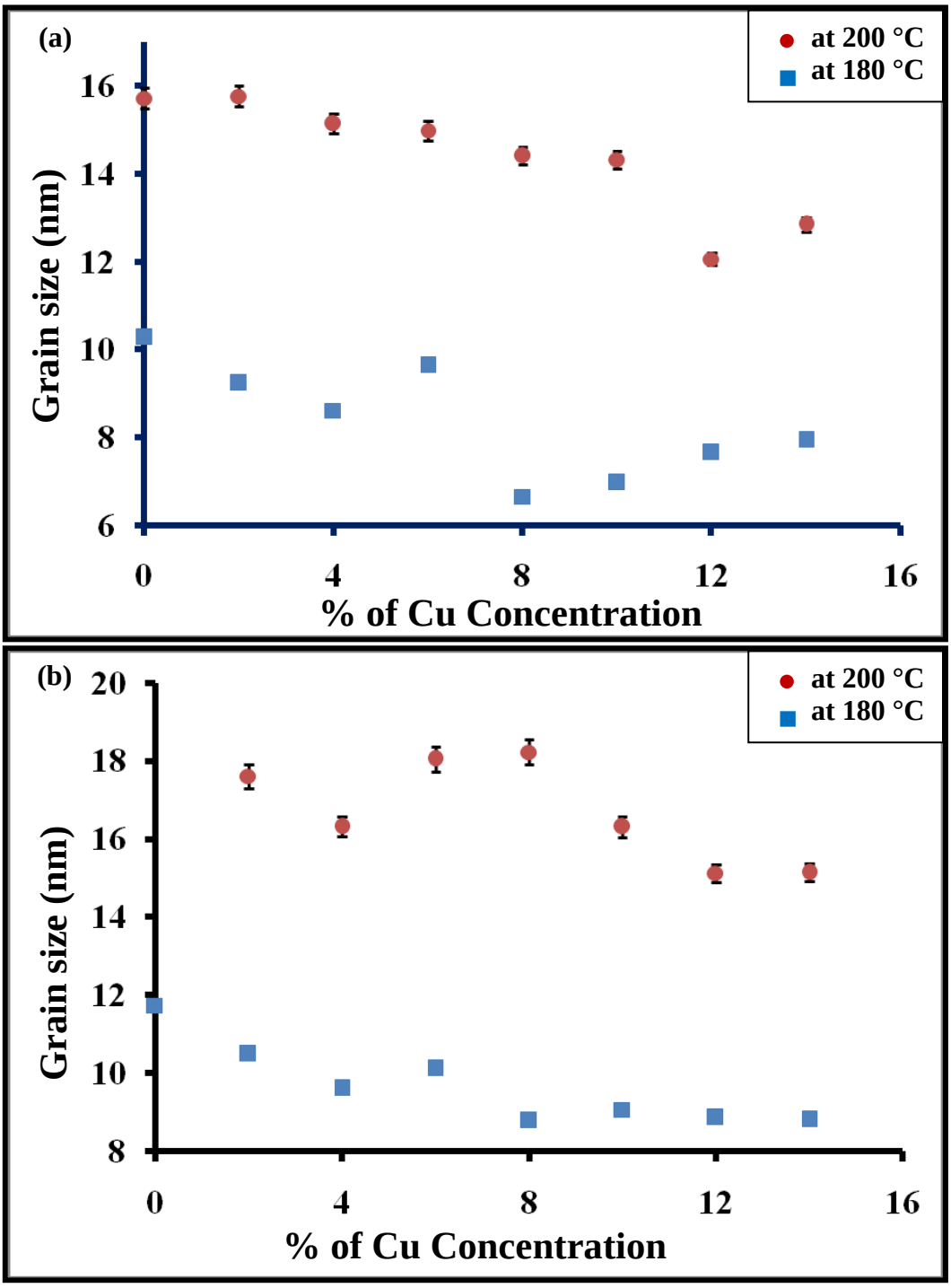

Figure 5-14 The grain size versus Cu concentration for $Zn_{1-x}Cu_xO$ synthesized by microwave assisted polyol method at temperatures of 180 ºC and 200 ºC for(a) 1% (b) 2% of precursor materials.

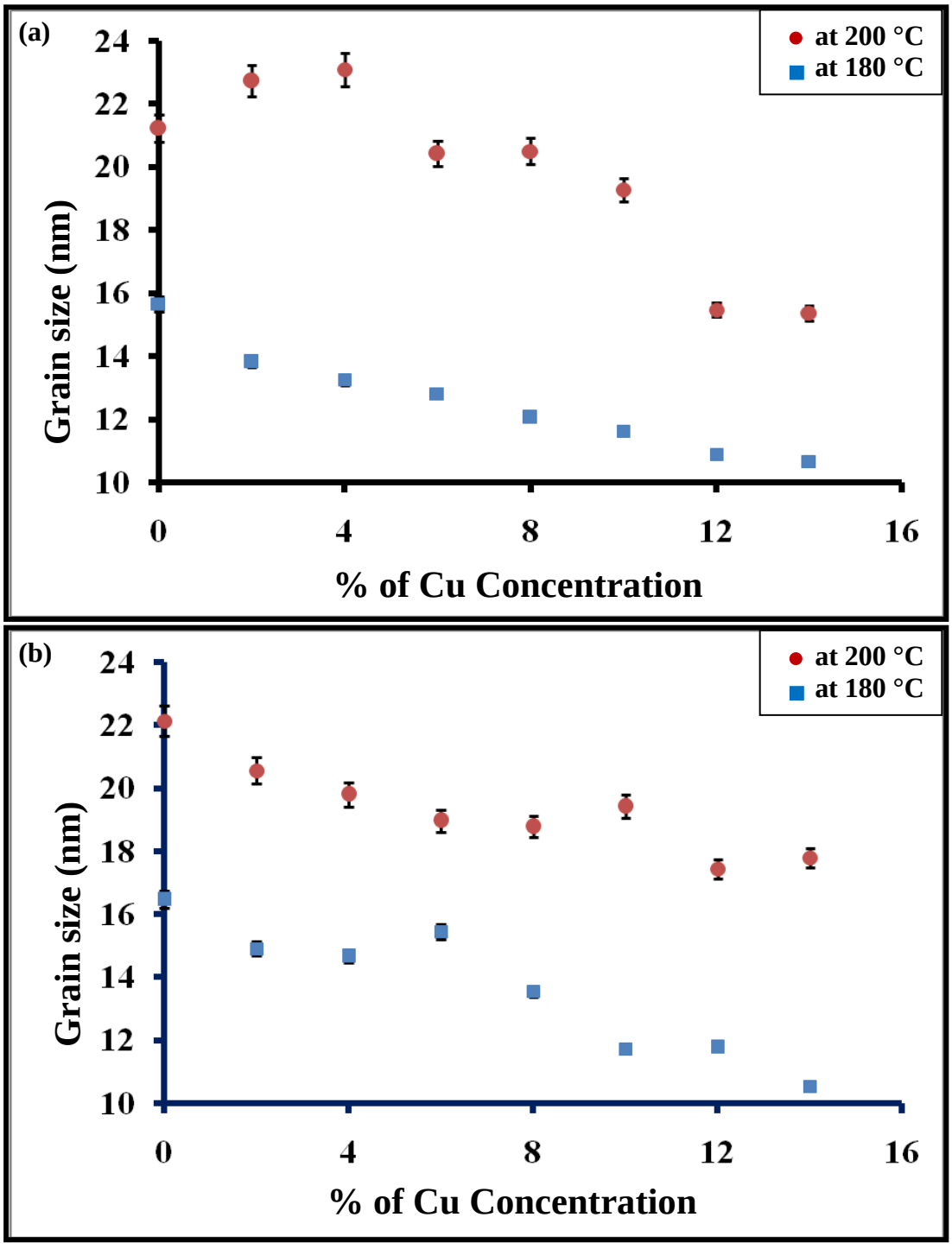

Figure 5-15 The grain size versus Cu concentration for $Zn_{1-x}Cu_xO$ synthesized by microwave assisted polyol method at temperatures of 180 ºC and 200 ºC for (a) 3% (b) 4% of precursor materials.

Figure 5-16 shows the relation between temperature and the grain size. One can clearly observe the increase the grain size with increasing temperature. The grain size has increased from 7 to 16 nm as temperature increased from 180 °C to 220 °C. This is attributed to increasing the growth of grains with rising temperature [72]. We could not expand the range of temperature. This is due to the decomposition of the sample does not occur at temperatures less than 180 °C whereas the solvent start evaporating at temperatures over 220 °C.

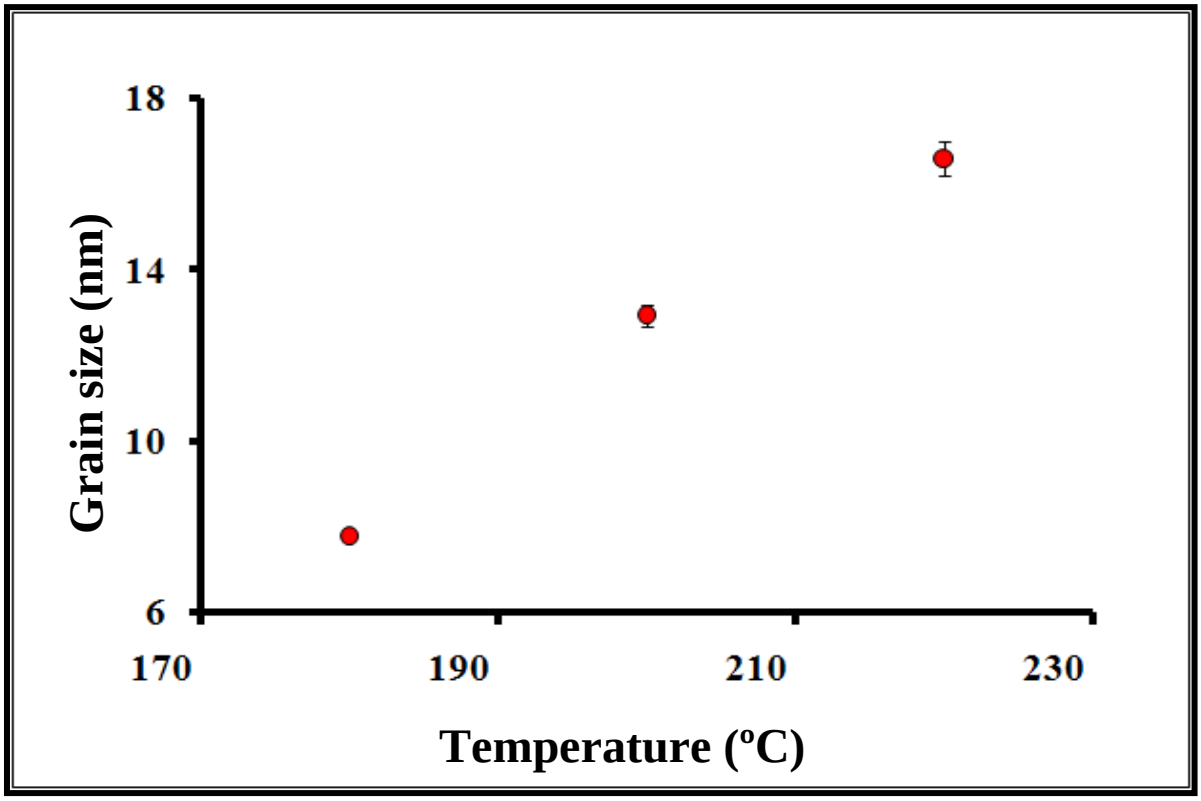

Figure 5-16 Effect of temperature on the grain size of ZnO nanopowders

5.2.2. XPS Results

Figures 5-17 and 5-18 exhibit the XPS spectra (0 – 1200 eV) of two samples of ($Zn_{1-x}OCu_x$, x=0.02and 0.10 respectively) synthesized at 180 °C. All elements that are shown within the spectra were ascribed to Zn, Cu, O and C according to XPS data handbook[68]

They show binding energies peaks of Zn, Cu and O for the two doped samples. The peaks of Zn and Cu were found at 2p3/2 and 2p1/2 whereas the O peak was observed at O1s.

The peaks 2p3/2 of Zn and Cu and the O1s peak of O were resolved into peaks for each one by Gaussian-Lorentz as shown from Figure 5-19 to Figure 5-24. The binding energy values of resolved peaks are recorded in Table 5-4.

Table 5-4 XPS spectra of binding energies of Cu-doped ZnO samples.

Sample	**Binding Energy of $Zn2p_{3/2}$ (eV) with components ratio**	**Binding Energy of O1s (eV) with components ratio**	**Binding Energy of $Cu2p_{3/2}$(eV) with components ratio**
$Zn_{0.98}OCu_{0.02}$	1021.29 (32.15%)	532.42 (8.97%)	934.02 (0.042%)
	1020.25 (20.55%)	530.83 (18.01%)	932.17 (0.601%)
	- - - - - -	529.26 (19.54%)	930.36 (0.143%)
$Zn_{0.90}OCu_{0.10}$	1024.04 (19.8%)	532.44 (1.414%)	936.33 (0.258%)
	1023.11 (42.5%)	530.83 (6.78%)	935.09 (0.512%)
	1021.09 (8.3%)	529.03 (19.08%)	934.03 (1.331%)

Table 5-4 shows that Zn^{+2} in $Zn_{0.98}OCu_{0.02}$ and $Zn_{0.90}OCu_{0.10}$ has binding energies at 1021.29 and 1023.11eV, respectively whereas the rest of binging energies peaks were attributed to unknown components of Zn. As can be seen Cu^{+2} binding energies were located at 934.02eV and 934.03eV for $Zn_{0.98}OCu_{0.02}$ and $Zn_{0.90}OCu_{0.10}$ respectively while Cu^{+1} has only the binding energy at 932.17eV within $Zn_{0.98}OCu_{0.02}$ sample. The other binding energies, 930.36, 936.33 and 935.09 eV of the two samples belong to unknown components for Cu [69–71].

The O1s peak has been resolved into three binding energies for each Cu-doped sample as shown in Table5-4. The lower peaks (529.26 and 529.03eV) for two samples were ascribed to oxygen deficient regions respectively while the higher peaks (532.42 and 532.44eV) belong to loosely bound oxygen, such as OH bond, existing on the surface of the sample respectively. The middle peaks (530.83eVof both samples) are attributed to O^{-2} ions related to O^{-2} ions in ZnO lattice[78–80].

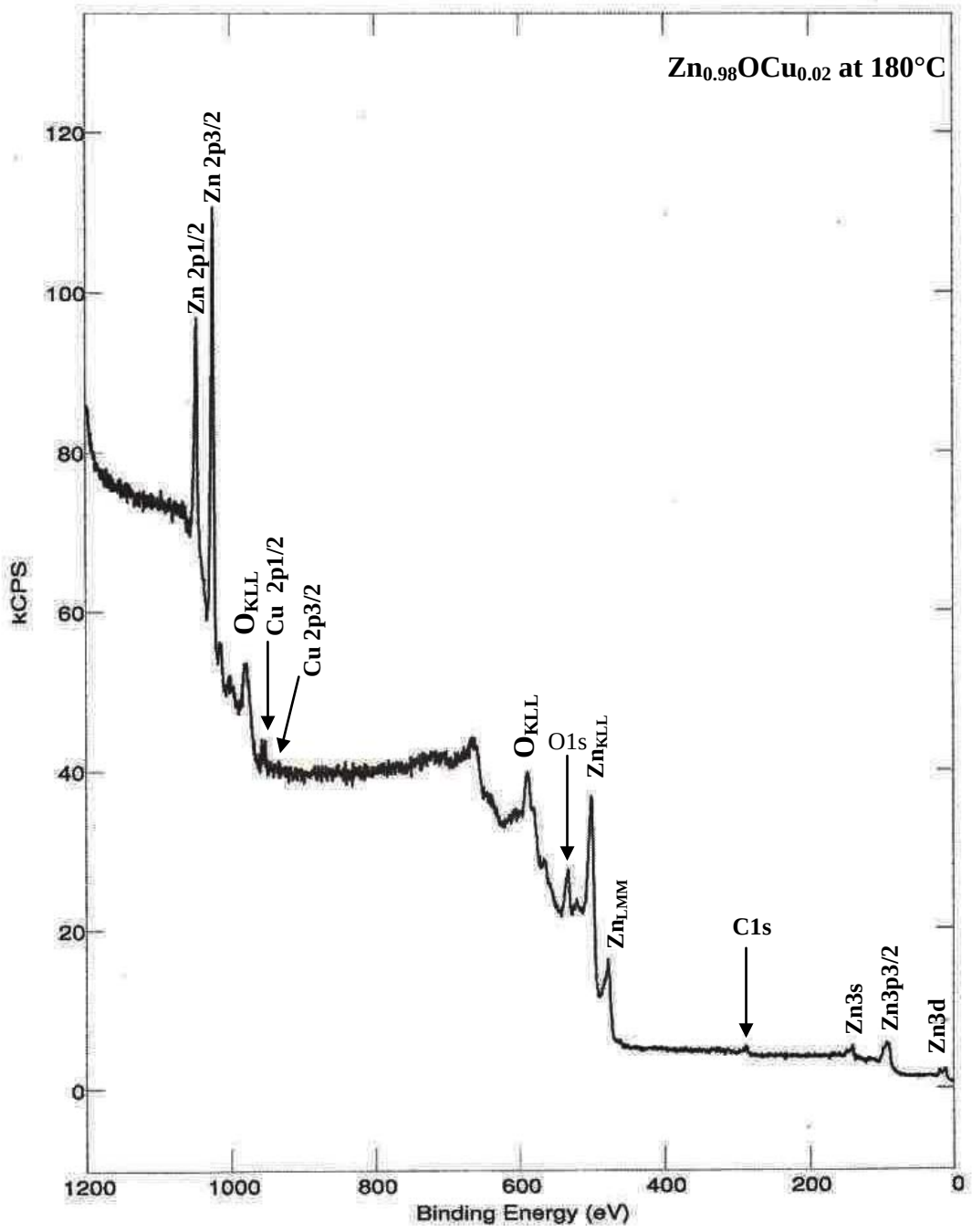

Figure 5-17 XPS spectrum of $Zn_{0.98}OCu_{0.02}$ synthesized at 180 °C by microwave assisted polyol method, showing the binding energy peaks corresponding to Zn 2p, Cu 2p, O 1s and C 1s.

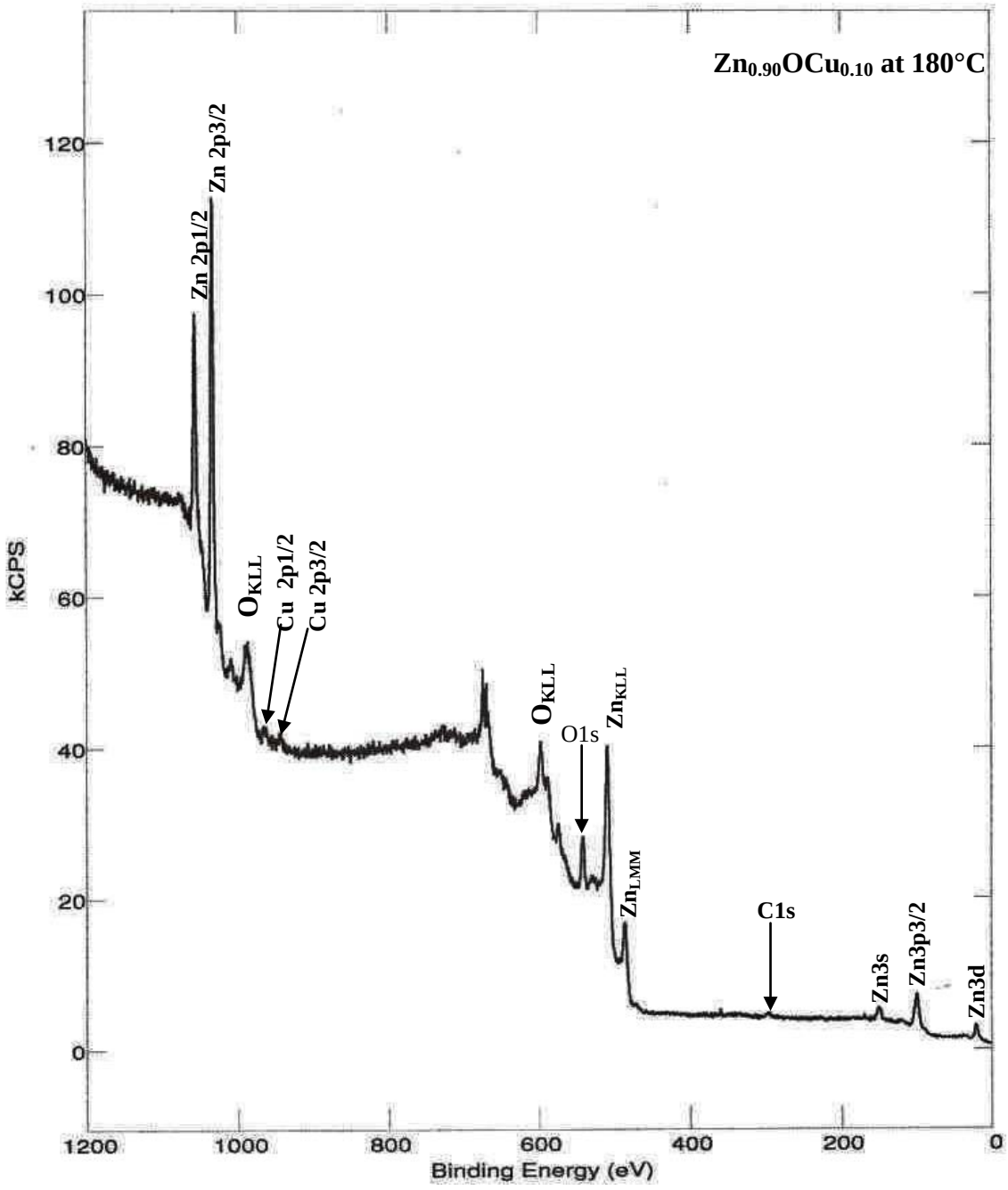

Figure 5-18 XPS spectrum of $Zn_{0.90}OCu_{0.10}$ synthesized at 180 °C by microwave assisted polyol method, showing the binding energy peaks corresponding to Zn 2p, Cu 2p, O 1s and C 1s

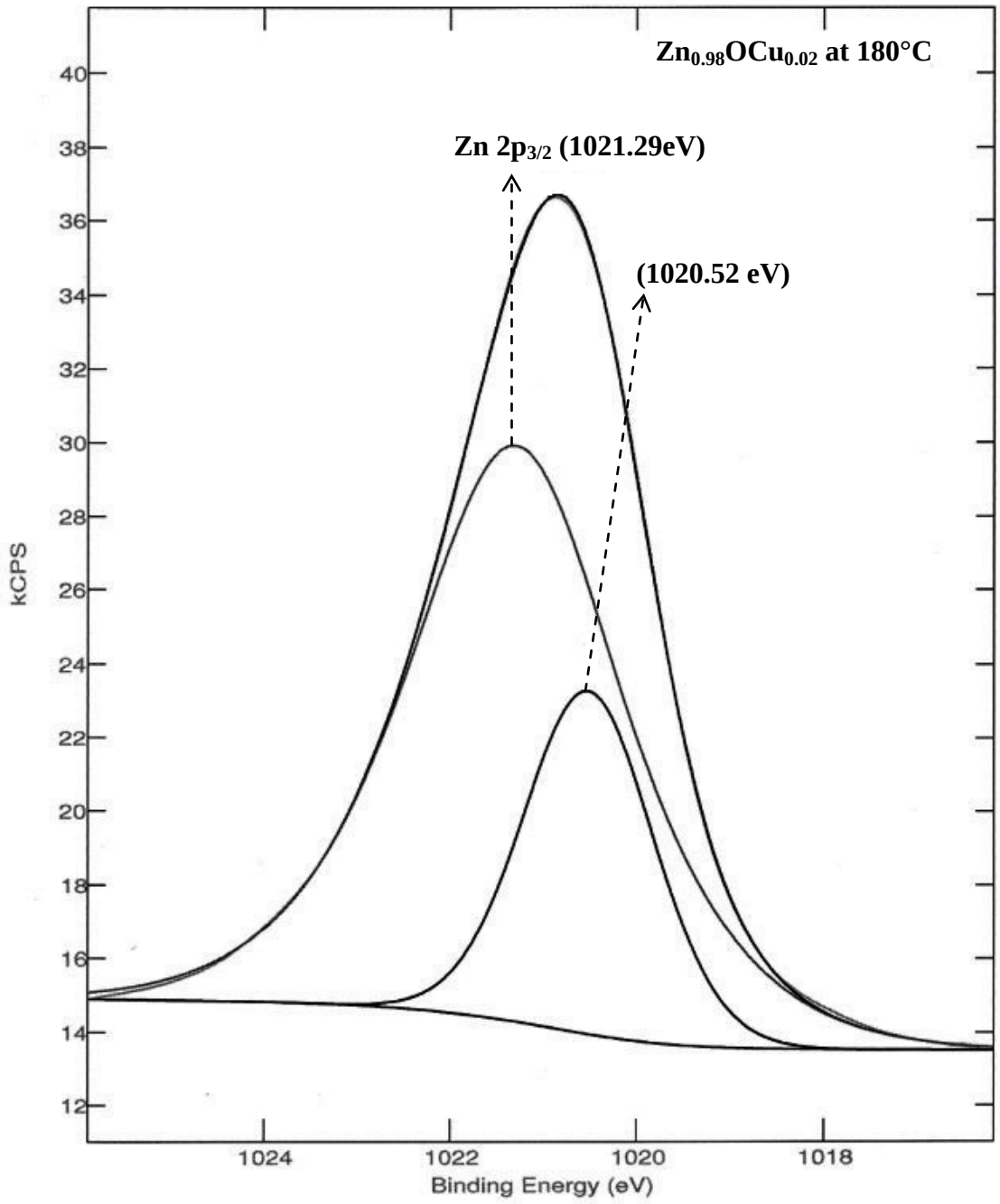

Figure 5-19 Resolving the binding energy peak of Zn $2p_{3/2}$ into two peaks for $Zn_{0.98}OCu_{0.02}$ synthesized at 180 °C.

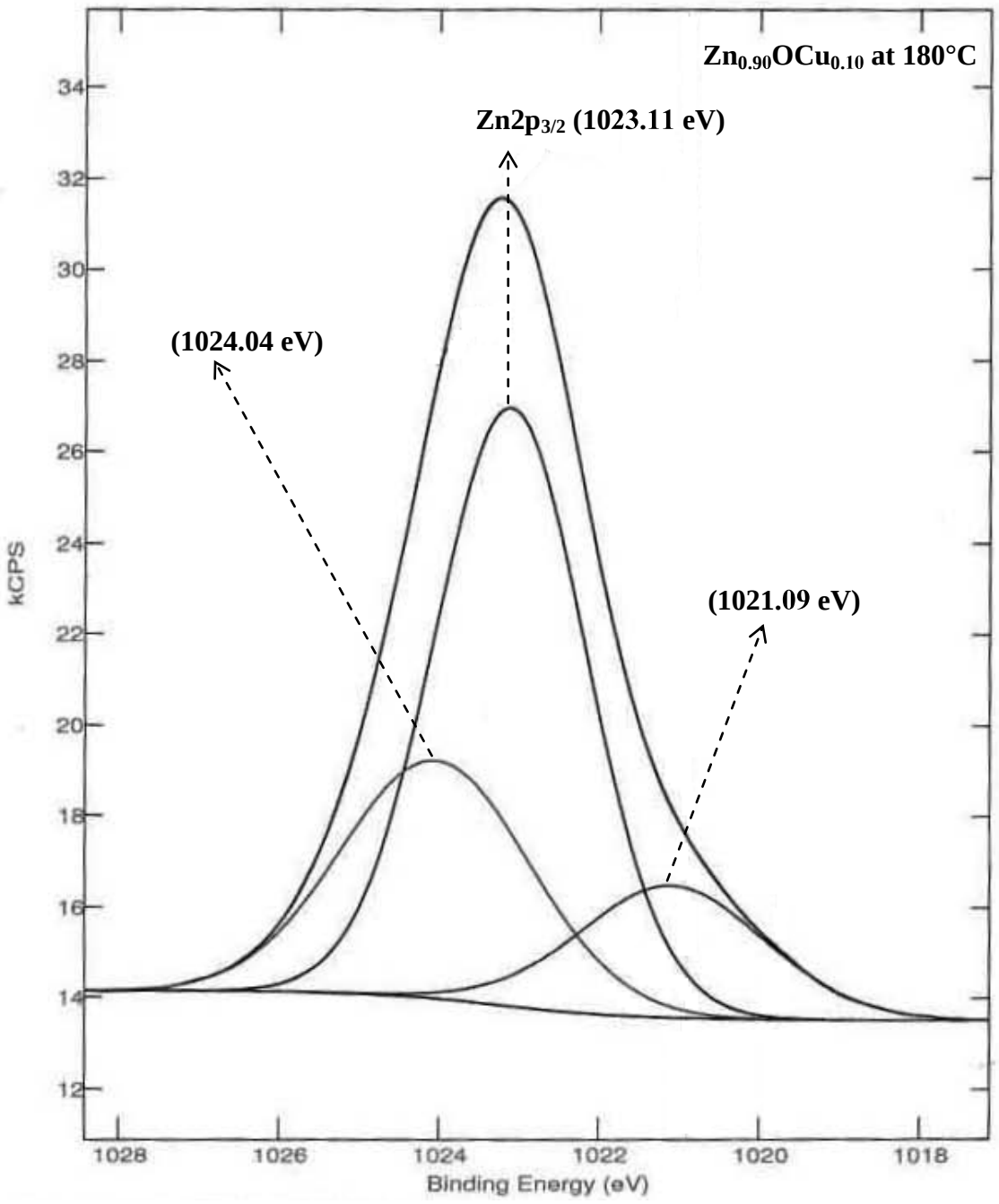

Figure 5-20 Resolving the binding energy peak of Zn $2p_{3/2}$ into three peaks for $Zn_{0.90}OCu_{0.10}$ synthesized at 180 °C.

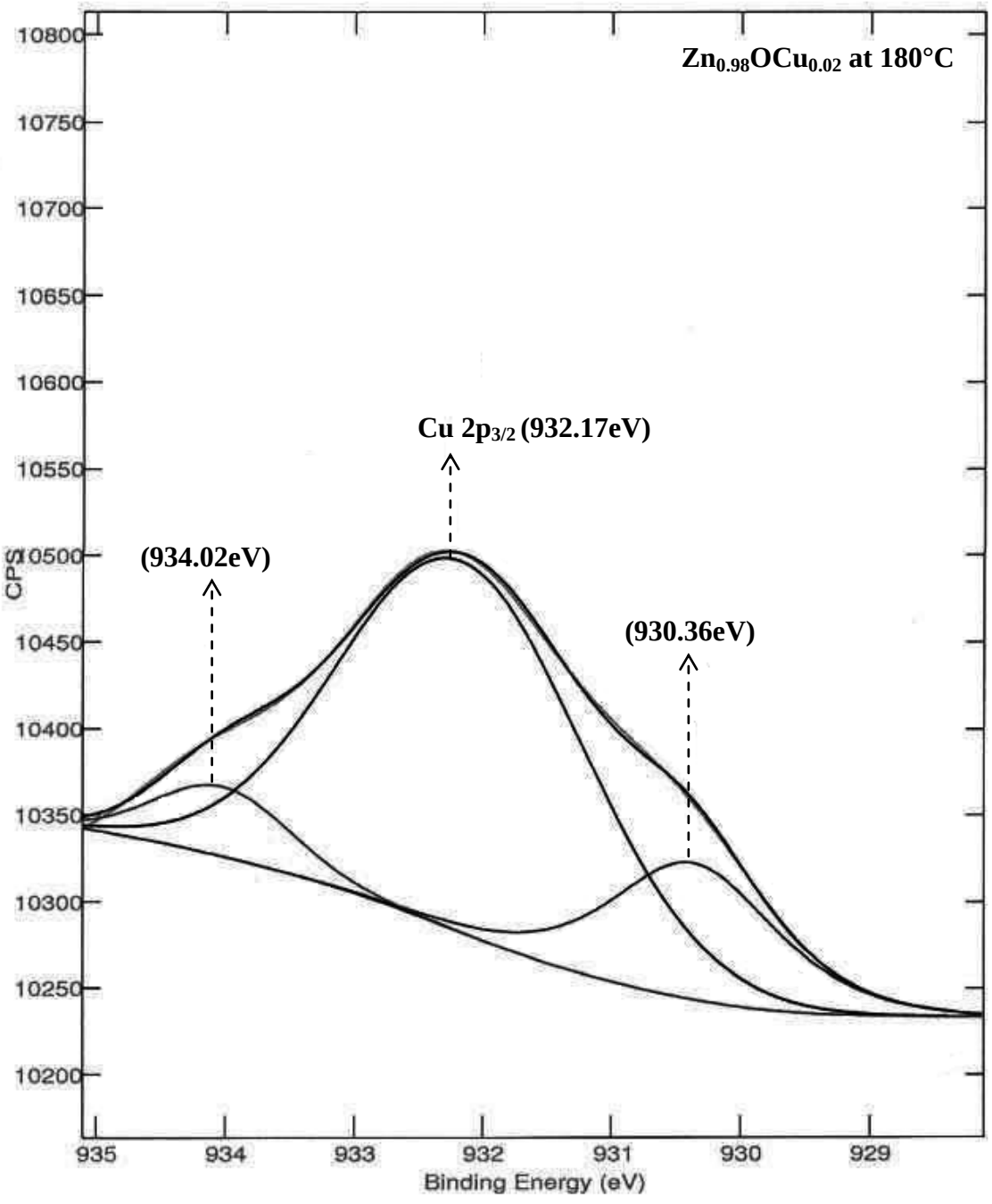

Figure 5-21 Resolving the binding energy peak of Cu $2p_{3/2}$ into three peaks for $Zn_{0.98}OCu_{0.02}$ synthesized at 180 °C.

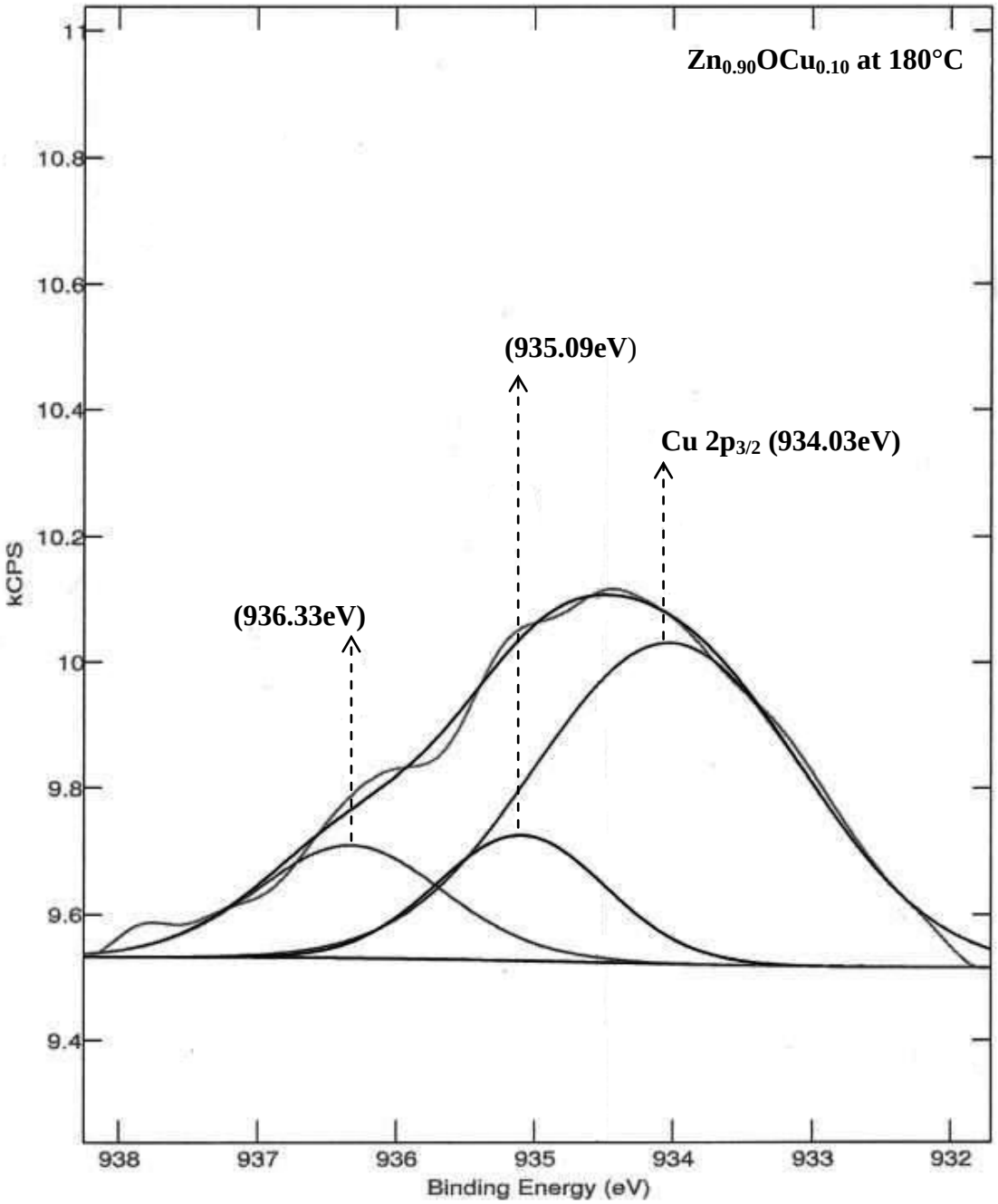

Figure 5-22 Resolving the binding energy peak of Cu $2p_{3/2}$ into three peaks for $Zn_{0.90}OCu_{0.10}$ synthesized at 180 °C.

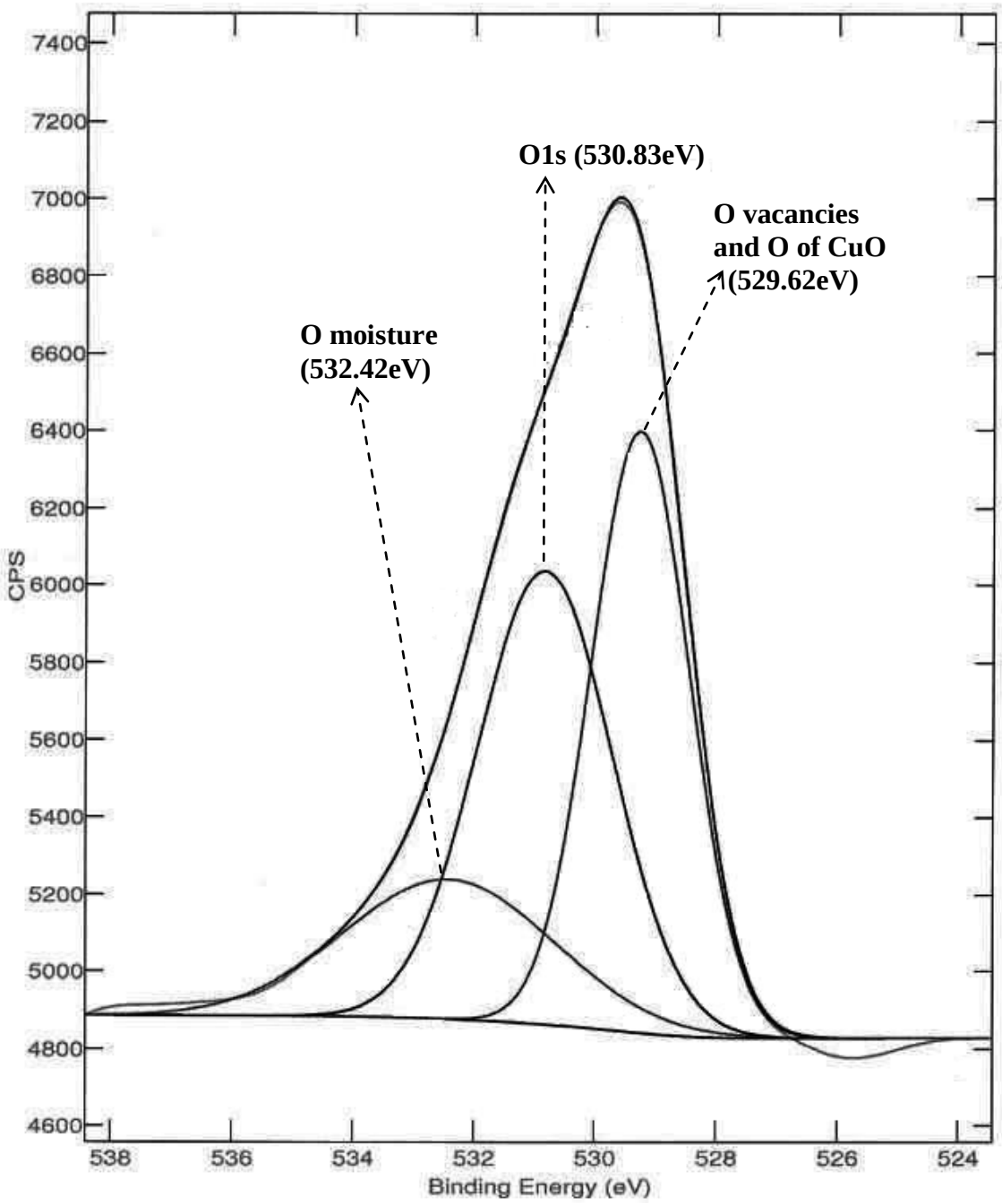

Figure 5-23 Resolving the binding energy peak of O 1s into three peaks for $Zn_{0.98}OCu_{0.02}$ synthesized at 180 °C.

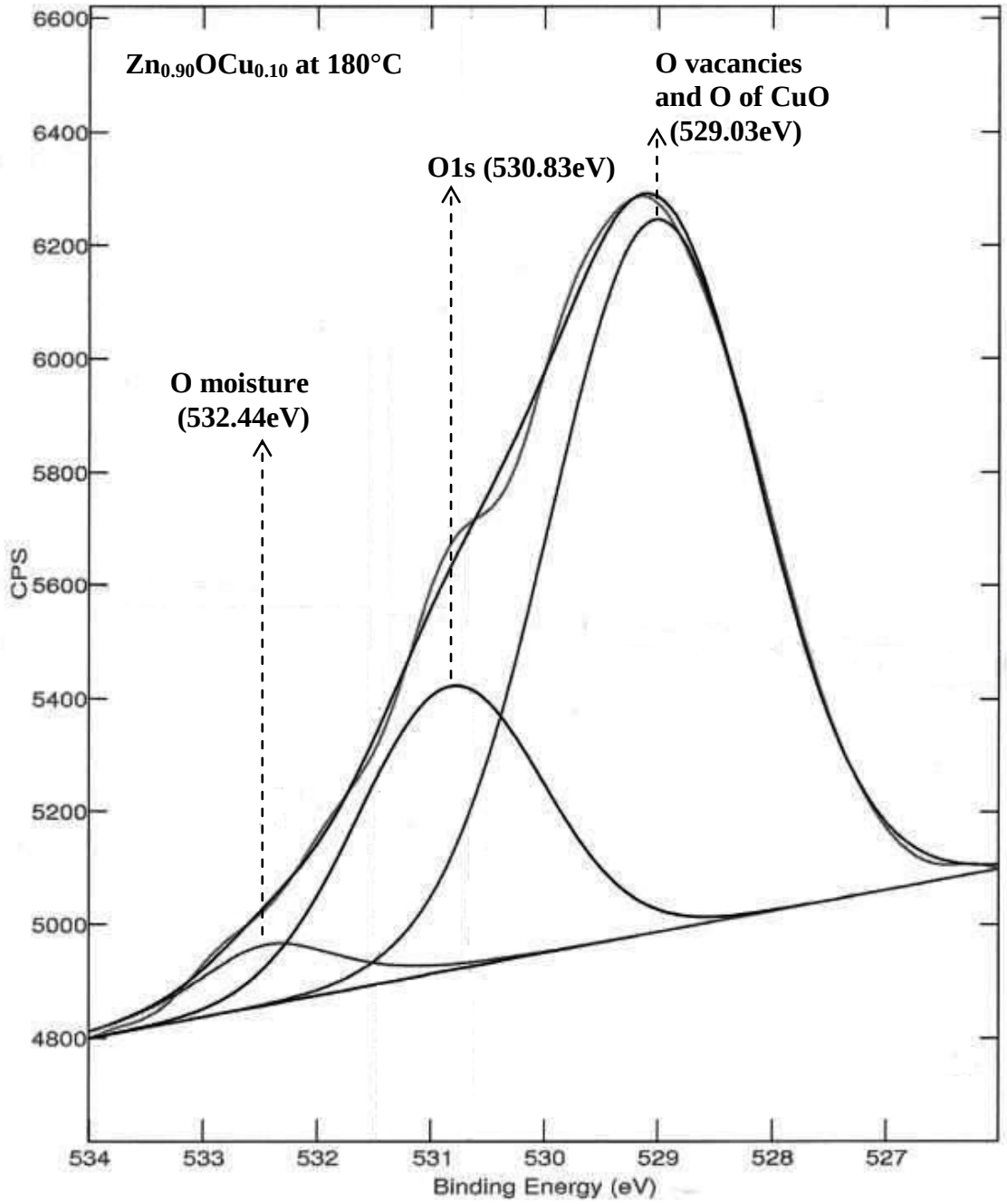

Figure 5-24 Resolving the binding energy peak of O 1s into three peaks for $Zn_{0.90}OCu_{0.10}$ synthesized at 180 °C.

5.2.3. FESEM results

Figures 5-25, 5-26, 5-27 and 5-28 represent typical FESEM images taken for four samples synthesized by microwave assisted polyol method at two different temperatures. Figures 5-25 and 5-26 show the morphology for pure samples of ZnO at temperature 180°C and 200°C while Figures 5-27 and 5-28 represent the morphology of $Zn_{0.86}Cu_{0.14}O$ at temperature 180 °C and 200 °C. Each figure includes three images; a and b at low magnification whereas c at high magnification. All samples show that the morphology of ZnO nanostructure did not change after doping ZnO with Cu. The morphology of the samples exhibited large spherical particles with diameter ranging from 400 to750 nm were formed by agglomeration of ZnO nanoparticles as shown in all figures at (a) and (b). It can be seen the nanoparticles located on the surface of these particles as grains with sizes in several nanometers. Influence of temperature on the morphology increased agglomerating nanoparticles as shown in Figures 5-26 and 5-28.

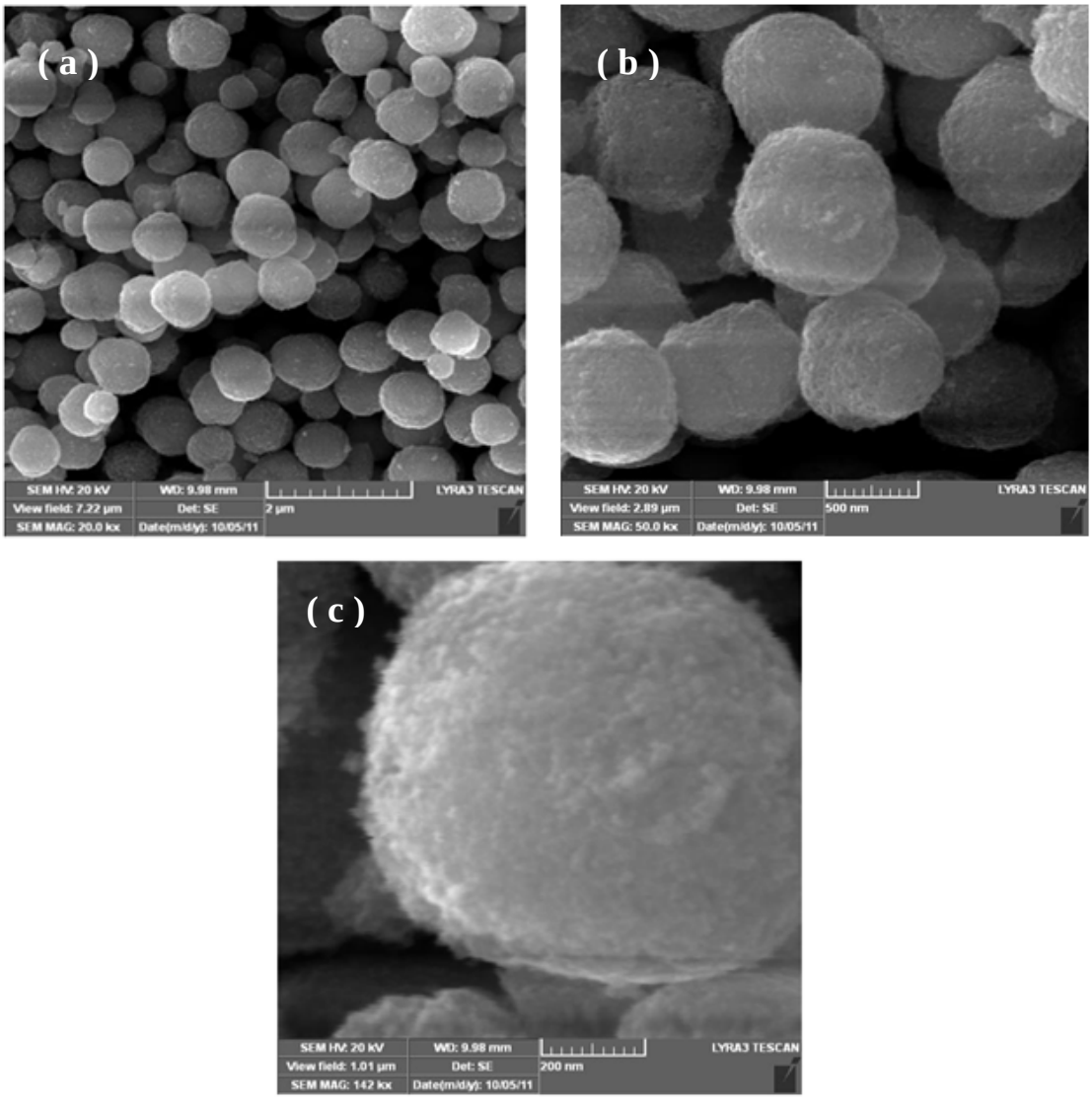

Figure 5-25 Morphology of a pure sample of ZnO synthesized at temperature of 180 °C via microwave assisted polyol method

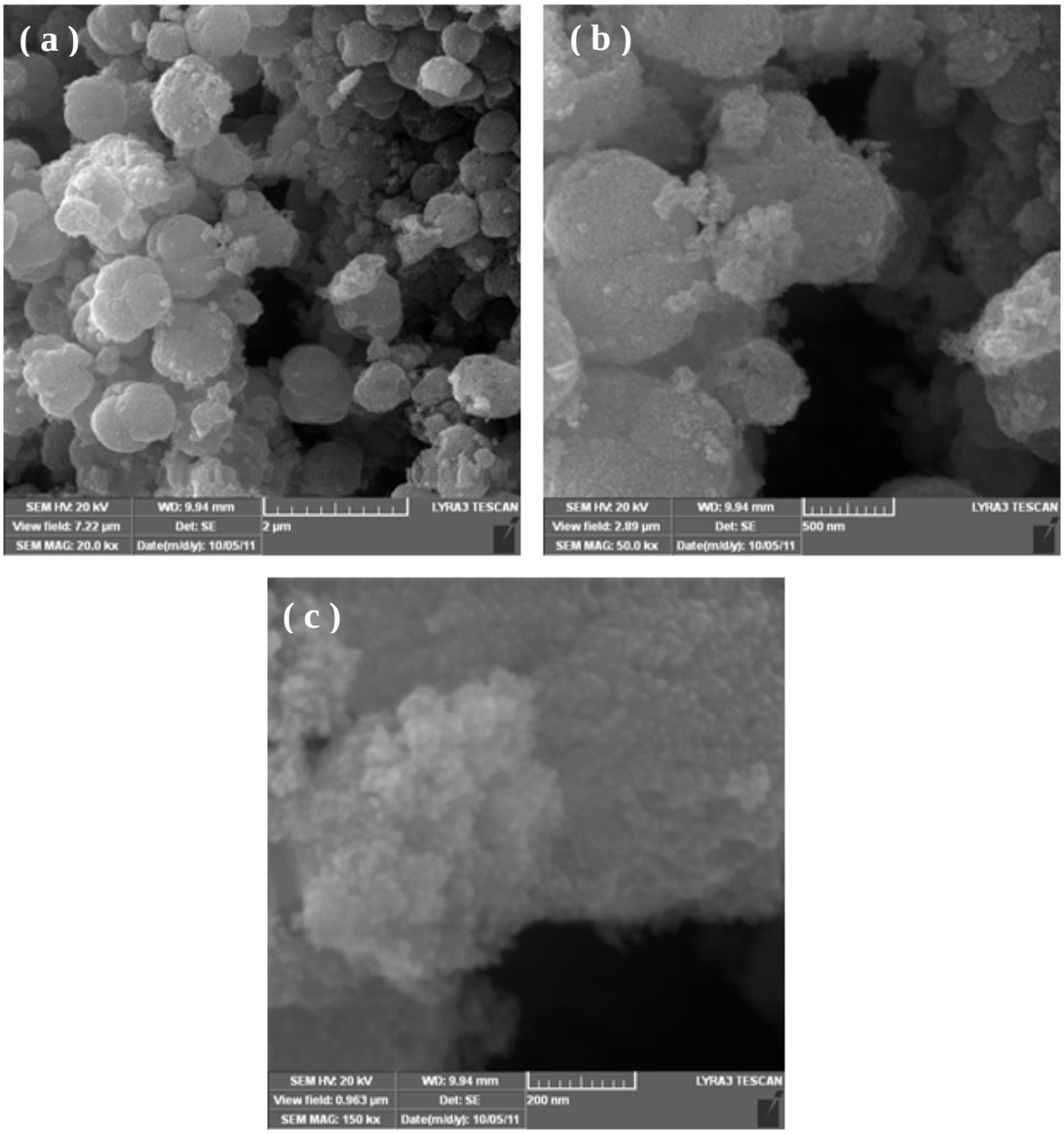

Figure 5-26 Morphology of a pure sample of ZnO synthesized at temperature of 200 °C via microwave assisted polyol method.

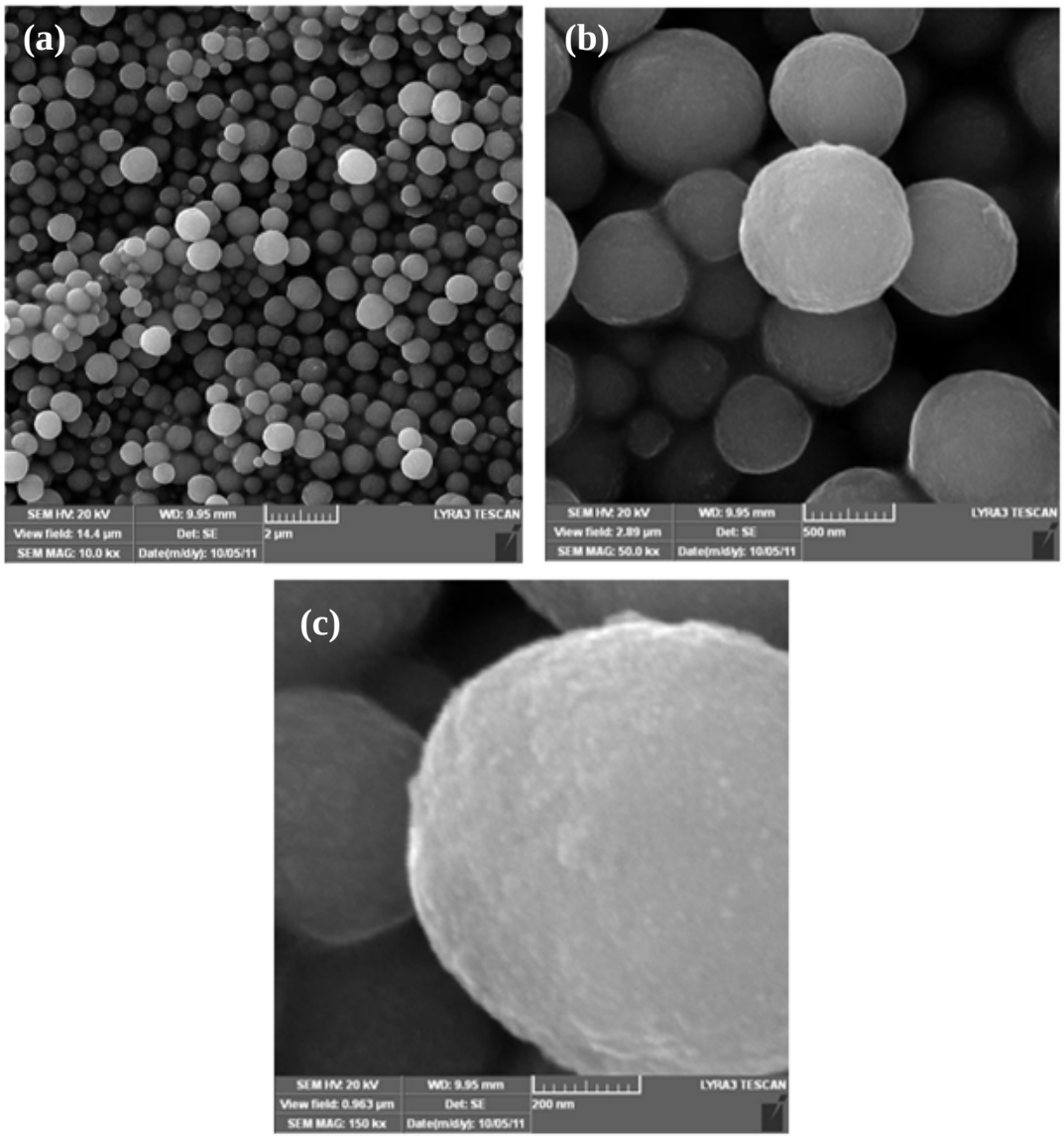

Figure 5-27 Morphology of $Zn_{0.86}OCu_{0.14}$ synthesized at temperature of 180 °C via microwave assisted polyol method

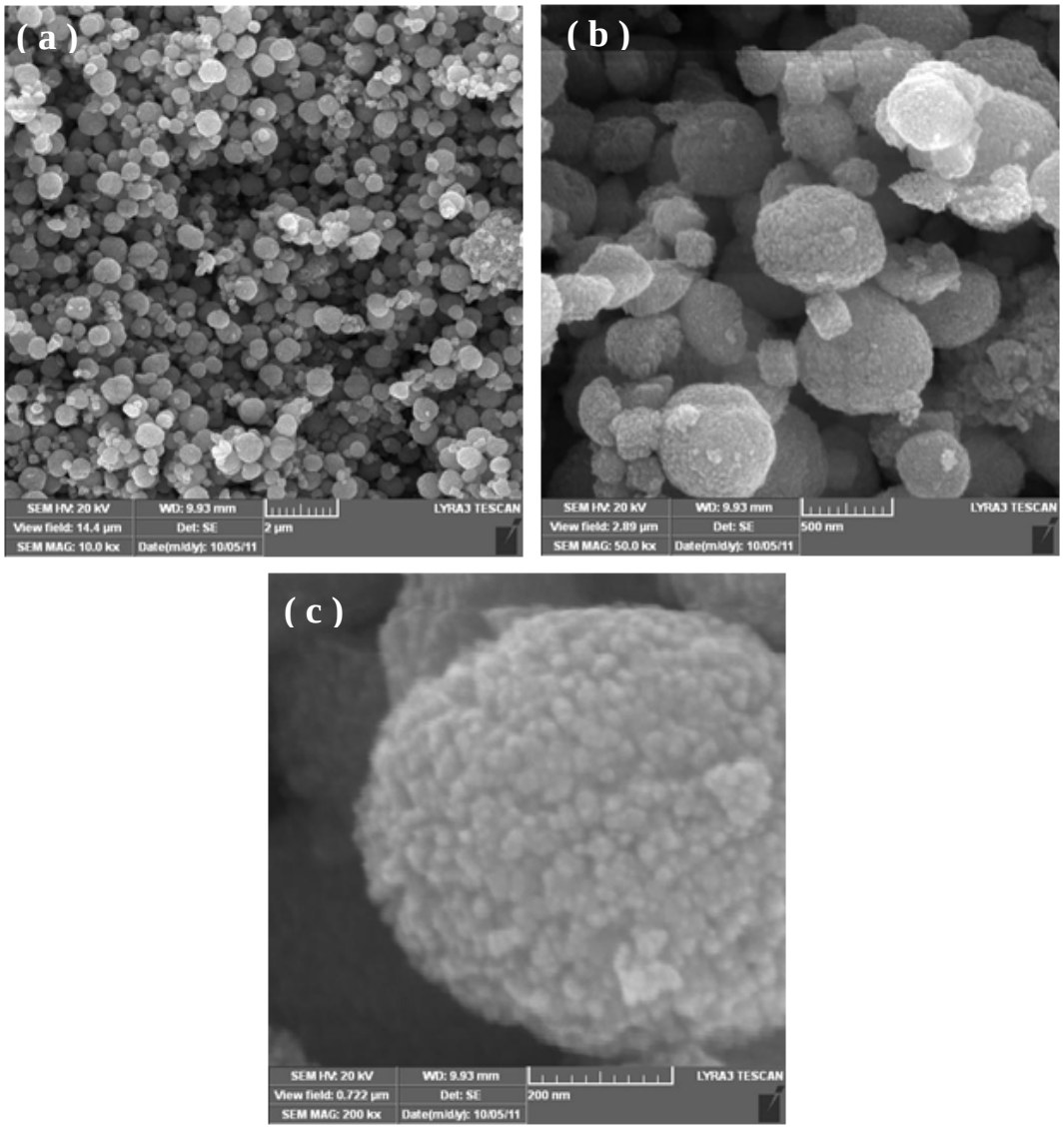

Figure 5-28 Morphology of $Zn_{0.86}OCu_{0.14}$ synthesized at temperature of 200 °C via microwave assisted polyol method.

5.2.4. EDS results

Figures5-29 and 5-30 show the spectra of EDS for the pure and doped samples synthesized by microwave assisted polyol method at two temperatures 180°C and 200°C, respectively. The chemical composition of samples indicates two components; Zn and O for pure samples whereas three components; Zn, Cu and O for doped ZnO samples and C peak coming from the tape was used to fix the sample. The spectrum emphasizes clearly the purity of the samples from other impurities.

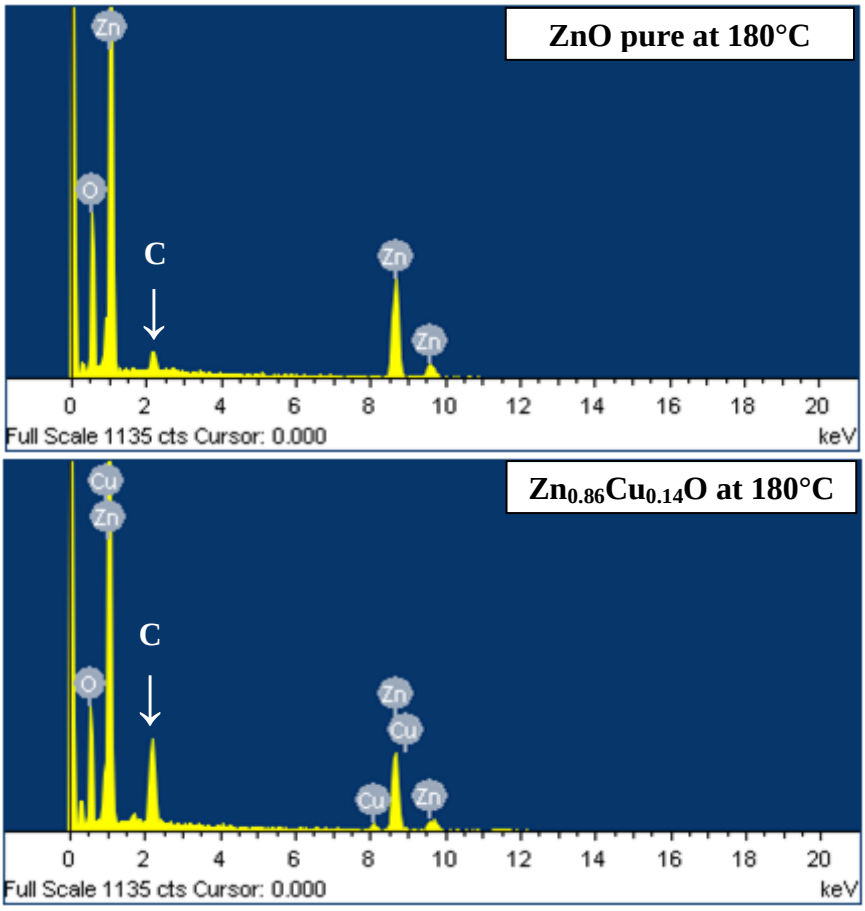

Figure 5-29 Spectrum and table showing the chemical purity and components ratios of pure ZnO and doped ZnO ($Zn_{0.86}OCu_{0.14}$) synthesized via microwave assisted polyol method at 180 °C.

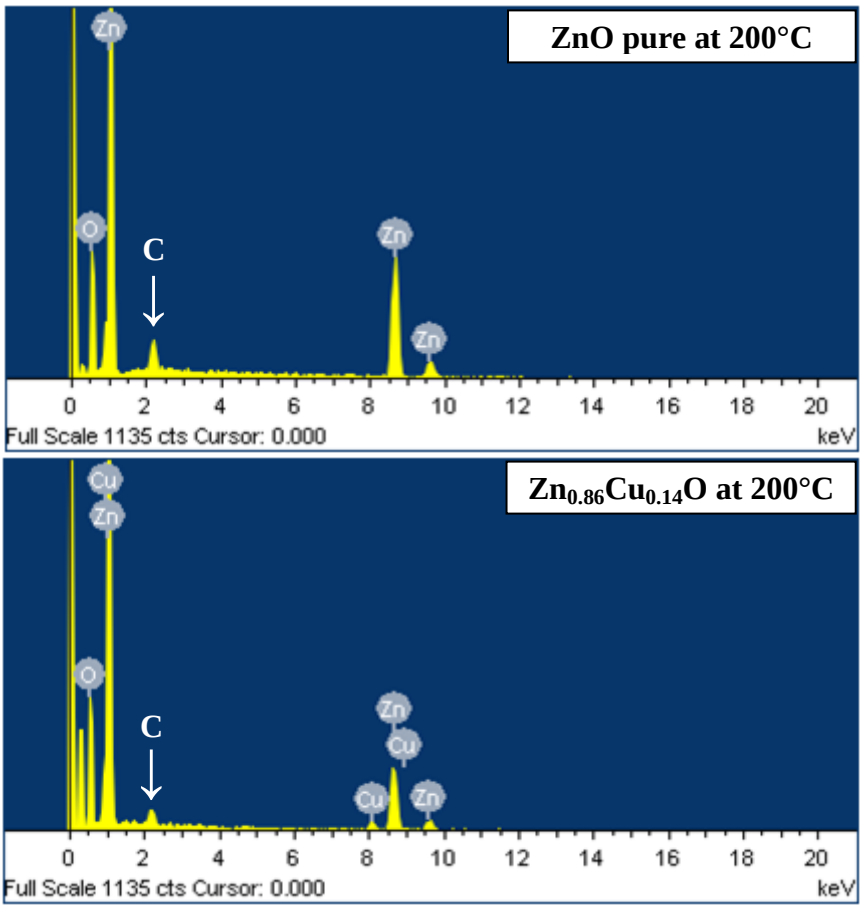

Figure 5-30 Spectrum and table showing the chemical purity and components ratios of pure ZnO and doped ZnO ($Zn_{0.86}OCu_{0.14}$) synthesized via microwave assisted polyol method at 200 °C

5.2.5. UV-visible diffuse reflectance spectroscopy results:

Figure 5-31 exhibits the correlation between $(KE)^2$ versus E (photon energy) that represents Tauc's relation[67]

$$[K\,E]^2 = C_2(E - E_g)$$

where K Kubelka Munk absorption coefficient, C is constant, $E = h\nu$ is Photon energy, E_g is the band gap energy.

To estimate the band gap energy, the straight line of the exhibited curve on Figure 5-31 is extrapolated to the intersection point with E axis where $(KE)^2 = 0$. According to Tauc's relation E will be equal to the band gap energy(E_g).

The values of band gap energy were recorded in Table 5-5. It shows that the energy band gap energy of pure and doped ZnO decreased slightly from 3.29 to 3.25 eV as the Cu doping concentrations increases from 0.00 to 0.14 Cu.

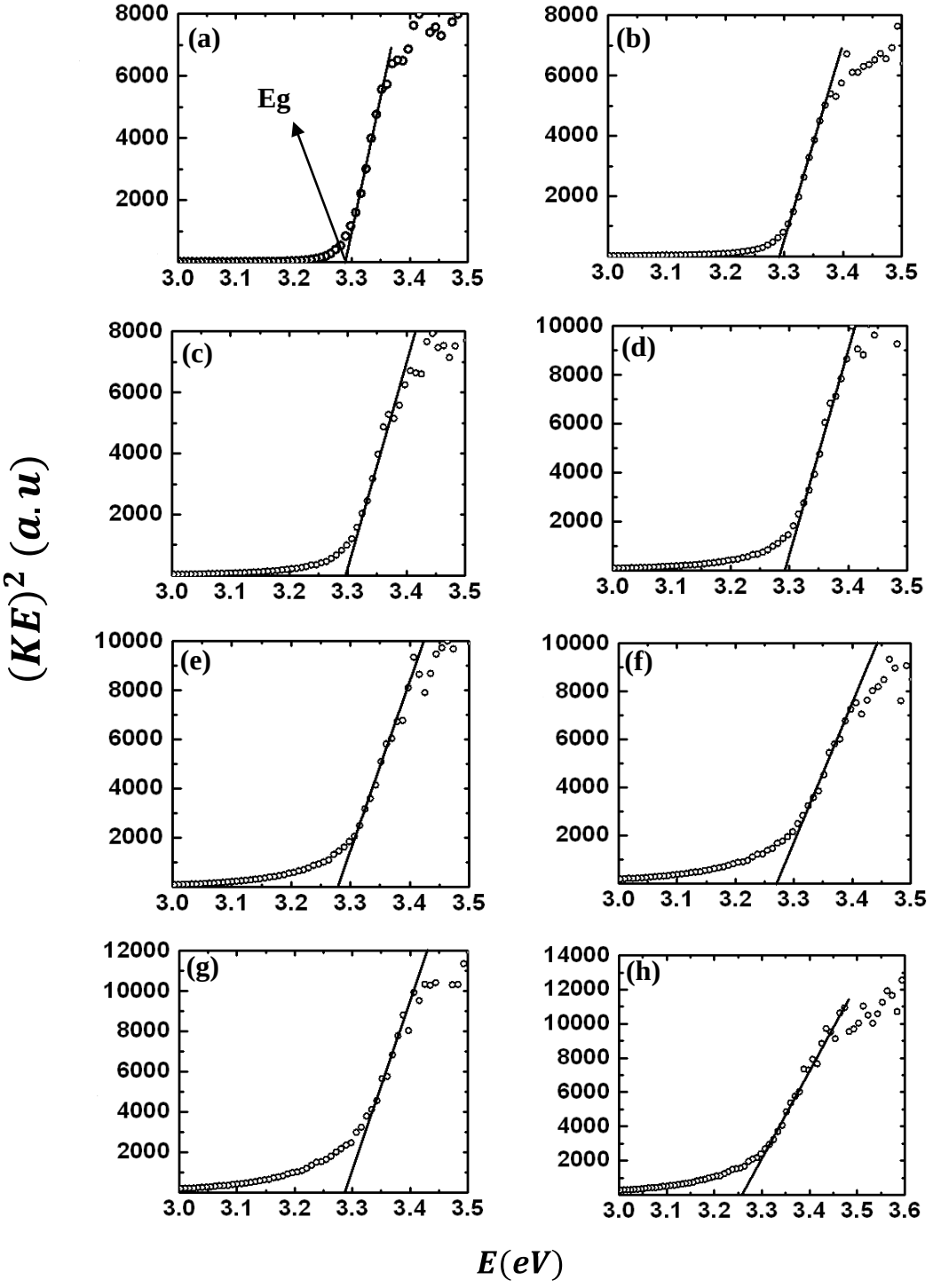

Figure 5-31 Estimate of the direct band gap for the samples (a) Pure ZnO (b) $Zn_{0.98}OCu_{0.02}$ (c) $Zn_{0.96}OCu_{0.04}$ (d) $Zn_{0.94}OCu_{0.06}$ (e) $Zn_{0.92}OCu_{0.08}$ (f) $Zn_{0.90}OCu_{0.10}$ (g) $Zn_{0.88}OCu_{0.12}$ (h) $Zn_{0.86}OCu_{0.14}$ synthesized at 180 °C by microwave assisted polyol method.

Table 5-5 Estimated values of energy band gap for Cu-doped ZnO samples ($Zn_{1-x}Cu_xO$)

Sample	Estimated energy band gap (eV)
ZnO	3.29
$Zn_{0.98}Cu_{0.02}O$	3.29
$Zn_{0.96}Cu_{0.04}O$	3.29
$Zn_{0.94}Cu_{0.06}O$	3.28
$Zn_{0.92}Cu_{0.08}O$	3.27
$Zn_{0.90}Cu_{0.10}O$	3.26
$Zn_{0.88}Cu_{0.12}O$	3.26
$Zn_{0.86}Cu_{0.14}O$	3.26

CHAPTER 6

CONCLUSION

In summary, ZnO nanopowders doped with different concentrations of Cu was synthesized by microwave assisted polyol methods. The domestic microwave oven was modified for synthesizing ZnO nanopowder. ZnO nanopowder was synthesized at temperatures of 180 ºC and 200 ºC. The structure, morphology, size and optical properties of the synthesized samples were characterized by analytical techniques such as XRD, XPS, FESEM, EDS and UV-visible Spectroscopy.

XRD results showed that the hexagonal structure of ZnO did not change after doping by Cu. The grain size increased with increasing temperature whereas it decreased with increasing Cu doping concentration. The lattice parameters of ZnO had little change in the doped samples.

XPS results emphasized the presence of Cu^{+2} within Zn^{+2} crystals and EDS spectra clearly confirmed the chemical purity of the investigated samples.

FESEM investigation of pure ZnO and Cu-doped ZnO synthesized by microwave assisted polyol method at 180 ºC and 200 ºC revealed that the shape of particles was spherical and these particles consisted of agglomeration of nanoparticles. The shape of

particles of samples synthesized at 180ºC had a spherical shape more regular than those samples synthesized at 200ºC.

The results of UV –visible diffuse reflectance spectroscopy showed that the energy band gap of synthesized ZnO decreases only slightly from 3.29 to 3.26 eV with increasing Cu doping concentration within the ZnO samples

.

REFERENCES

[1] K. S. Gandhi, "Nanoscience and Technology: A Chemical Engineer's Perspective," *Engineer*, vol. 49, no. 3, pp. 251-266, 2007.

[2] E. Roduner, "Size matters: why nanomaterials are different," *The Royal Society of Chemistry*, vol. 35, pp. 583–592, 2006.

[3] N. S. Pesika, K. J. Stebe, and P. C. Searson, "Relationship between Absorbance Spectra and Particle Size Distributions for Quantum-Sized Nanocrystals," *Society*, pp. 10412-10415, 2003.

[4] N. Lepot et al., "Synthesis of ZnO nanorods from aqueous solution," *Materials Letters*, vol. 61, no. 13, pp. 2624-2627, 2007.

[5] M. T. Swihart, "Vapor-phase synthesis of nanoparticles," *Current opinion in colloid & interface science*, vol. 8, no. 1, pp. 127–133, 2003.

[6] M. B. Ward, R. Brydson, and R. F. Cochrane, "Mn nanoparticles produced by inert gas condensation," *Journal of Physics: Conference Series*, vol. 26, pp. 296-299, 2006.

[7] L. C. Damonte, L. a. Mendoza Zélis, B. Marí Soucase, and M. a. Hernández Fenollosa, "Nanoparticles of ZnO obtained by mechanical milling," *Powder Technology*, vol. 148, no. 1, pp. 15-19, 2004.

[8] B. Liu and H. C. Zeng, “Mesoscale organization of CuO nanoribbons: formation of ‘dandelions’.,” *Journal of the American Chemical Society*, vol. 126, no. 26, pp. 8124-5, 2004.

[9] T. Guo, P. Nikolaev, A. G. Rinzler, D. Tombnek, D. T. Colbert, and R. E. Smalley, “Self-Assembly of Tubular Fullerenes,” pp. 10694-10697, 1995.

[10] B. A. Nejand, S. Sanjabi, and V. Ahmadi, “The effect of sputtering gas pressure on structure and photocatalytic properties of nanostructured titanium oxide self-cleaning thin film,” *Vacuum*, vol. 85, no. 3, pp. 400-405, 2010.

[11] M. Messing, “Gold Particles for Growth of Semiconductor Nanowires,” Lund University, 2009.

[12] W. Nimmo, N. J. Ali, R. Brydson, C. Calvert, and S. J. Milne, “Particle Formation During Spray Pyrolysis of Lead Zirconate Titanate,” *Journal of the American Ceramic Society*, vol. 88, no. 4, pp. 839-844, 2005.

[13] W. Nimmo, D. Hind, N. J. Ali, E. Hampartsoumian, and S. J. Milne, “The production of ultrafine zirconium oxide powders by spray pyrolysis,” vol. 7, pp. 3381-3387, 2002.

[14] F. Mafune, J.-ya Kohno, Y. Takeda, and T. Kondow, “Formation of Gold Nanoparticles by Laser Ablation in Aqueous Solution of Surfactant,” *Society*, pp. 5114-5120, 2001.

[15] T. Ohshima, T. Ikegami, K. Ebihara, and R. A. J. K. Thareja, “Photo-Excited Photonic Characteristics of ZnO Thin Films Deposited by Laser Ablation Method,” *Electrical Engineering*, vol. 144, no. 3, pp. 689-694, 2003.

[16] b M. I. and O. O. K. Kawasaki, a J. F. Despres, a S. Kamei, “Fabrication of nanometer-sized anatase particles by a pulsed laser ablation method,” *J. Mater. Chem.*, vol. 7, no. 10, pp. 2117-2120, 1997.

[17] I. Bertoti, I. Mohai, and J. Szepvolgyi, “Thermal plasma synthesis of zinc ferrite nanopowders,” *Solid State Ionics*, pp. 163-168, 2001.

[18] J. Heberlein, “New approaches in thermal plasma technology *,” *Symposium A Quarterly Journal In Modern Foreign Literatures*, vol. 74, no. 3, pp. 327-335, 2002.

[19] R. Mueller, “Nanoparticle synthesis at high production rates by flame spray pyrolysis,” *Chemical Engineering Science*, vol. 58, no. 10, pp. 1969-1976, 2003.

[20] N. Du, H. Zhang, B. Chen, J. Wu, D. Li, and D. Yang, “Low temperature chemical reaction synthesis of single-crystalline Eu(OH) 3 nanorods and their thermal conversion to Eu 2 O 3 nanorods,” *Nanotechnology*, vol. 18, no. 6, p. 065605, 2007.

[21] W. Qin, C. Yang, R. Yi, and G. Gao, “Hydrothermal Synthesis and Characterization of Single-Crystalline α-Fe2O3 Nanocubes,” *Journal of Nanomaterials*, vol. 2011, pp. 1-5, 2011.

[22] J. W. Choi, H. Y. Sohn, Y. J. Choi, and Z. Z. Fang, “Chemical vapor synthesis and characterization of aluminum nanopowder,” *Journal of Power Sources*, vol. 195, no. 5, pp. 1463-1471, 2010.

[23] J.-H. Pee, J.-C. Park, Y. Kim, K.-T. Hwang, and S. Kim, “Synthesis of porous nano-sized AlN by chemical vapor synthesis,” *Physica Scripta*, vol. 139, p. 014049, 2010.

[24] C. Chen, P. Liu, and C. Lu, “Synthesis and characterization of nano-sized ZnO powders by direct precipitation method,” *Chemical Engineering Journal*, vol. 144, no. 3, pp. 509-513, 2008.

[25] W. Jiang, X. Hua, Q. Han, X. Yang, L. Lu, and X. Wang, “Preparation of lamellar magnesium hydroxide nanoparticles via precipitation method,” *Powder Technology*, vol. 191, no. 3, pp. 227-230, 2009.

[26] L. Liu, J. Jiang, S. Jin, Z. Xia, and M. Tang, “Hydrothermal synthesis of β-bismuth oxide nanowires from particles,” *CrystEngComm*, vol. 13, no. 7, p. 2529, 2011.

[27] S. Feng and R. Xu, “New materials in hydrothermal synthesis.,” *Accounts of chemical research*, vol. 34, no. 3, pp. 239-47, 2001.

[28] K. Byrappa and T. Adschiri, “Hydrothermal technology for nanotechnology,” *Progress in Crystal Growth and Characterization of Materials*, vol. 53, no. 2, pp. 117-166, 2007.

[29] S.-eon Park, J.-san Chang, Y. K. Hwang, D. S. Kim, and S. H. Jhung, “Supramolecular interactions and morphology control in microwave synthesis of nanoporous materials,” *Young*, vol. 8, no. 2, 2004.

[30] E. Hammarberg, A. Prodi-schwab, and C. Feldmann, “Journal of Colloid and Interface Science Microwave-assisted polyol synthesis of aluminium- and indium-doped ZnO nanocrystals,” *Journal of Colloid And Interface Science*, vol. 334, no. 1, pp. 29-36, 2009.

[31] T. Krishnakumar, R. Jayaprakash, N. Pinna, V. N. Singh, B. R. Mehta, and a. R. Phani, “Microwave-assisted synthesis and characterization of flower shaped zinc oxide nanostructures,” *Materials Letters*, vol. 63, no. 2, pp. 242-245, 2009.

[32] John N. Laiena and D. A.Cleary, *Principles of Inorganic Materials Design*, 2nd ed. Wiley.

[33] Y. Ni, X. Cao, G. Wu, G. Hu, Z. Yang, and X. Wei, “Preparation, characterization and property study of zinc oxide nanoparticles via a simple solution-combusting method,” *Nanotechnology*, vol. 18, no. 15, p. 155603, 2007.

[34] L. P. Snedeker, A. S. Risbud, O. Masala, J. P. Zhang, and R. Seshadri, “Organic phase conversion of bulk (wurtzite) ZnO to nanophase (wurtzite and zinc blende) ZnO,” *Solid State Sciences*, vol. 7, no. 12, pp. 1500-1505, 2005.

[35] Z. L. Wang, “Zinc oxide nanostructures: growth, properties and applications,” *Journal of Physics: Condensed Matter*, vol. 16, no. 25, p. R829-R858, 2004.

[36] B. Liu and H. C. Zeng, “Hydrothermal synthesis of ZnO nanorods in the diameter regime of 50 nm.,” *Journal of the American Chemical Society*, vol. 125, no. 15, pp. 4430-1, 2003.

[37] S.-yuan Chu, T.-min Yan, and S.-li Chen, “Characteristics of sol-gel synthesis of ZnO-based powders,” vol. 9, pp. 349-352, 2000.

[38] V. V. Gafiychuk, B. K. Ostafiychuk, D. I. Popovych, I. D. Popovych, and a. S. Serednytski, “ZnO nanoparticles produced by reactive laser ablation,” *Applied Surface Science*, vol. 257, no. 20, pp. 8396-8401, 2011.

[39] N. L. Tarwal et al., “Photoluminescence of zinc oxide nanopowder synthesized by a combustion method,” *Powder Technology*, vol. 208, no. 1, pp. 185-188, 2011.

[40] a. B. Djurišić, a. M. C. Ng, and X. Y. Chen, "ZnO nanostructures for optoelectronics: Material properties and device applications," *Progress in Quantum Electronics*, vol. 34, no. 4, pp. 191-259, 2010.

[41] S. Venkatachalam, Y. Iida, and Y. Kanno, "Preparation and characterization of Al doped ZnO thin films by PLD," *Superlattices and Microstructures*, vol. 44, no. 1, pp. 127-135, 2008.

[42] M. L. Tu, Y. K. Su, and C. Y. Ma, "Nitrogen-doped p-type ZnO films prepared from nitrogen gas radio-frequency magnetron sputtering," *Journal of Applied Physics*, vol. 100, no. 5, p. 053705, 2006.

[43] W. Ao, J. Li, H. Yang, X. Zeng, and X. Ma, "Mechanochemical synthesis of zinc oxide nanocrystalline," *Powder Technology*, vol. 168, no. 3, pp. 148-151, 2006.

[44] S. Lee, S. Jeong, D. Kim, S. Hwang, M. Jeon, and J. Moon, "ZnO nanoparticles with controlled shapes and sizes prepared using a simple polyol synthesis," *Superlattices and Microstructures*, vol. 43, no. 4, pp. 330-339, 2008.

[45] D. Yiamsawas, K. Boonpavanitchakul, and W. Kangwansupamonkon, "Preparation of ZnO Nanostructures by Solvothermal Method," *Journal of Microscopy*, vol. 23, no. 1, pp. 75-78, 2009.

[46] N. Wang, L. Jiang, H. Peng, and G. Li, “Synthesis of ZnO nanostructures composed of nanosheets with controllable morphologies,” *Crystal Research and Technology*, vol. 44, no. 3, pp. 341-345, 2009.

[47] T. Tani, M. Lutz, and S. E. Pratsinis, “Homogeneous ZnO nanoparticles by flame spray pyrolysis,” pp. 337-343, 2002.

[48] Y. Ishikawa, Y. Shimizu, T. Sasaki, and N. Koshizaki, “Preparation of zinc oxide nanorods using pulsed laser ablation in water media at high temperature.,” *Journal of colloid and interface science*, vol. 300, no. 2, pp. 612-5, 2006.

[49] K. D. Bhatte, P. Tambade, S.-ichiro Fujita, M. Arai, and B. M. Bhanage, “Microwave-assisted additive free synthesis of nanocrystalline zinc oxide,” *Powder Technology*, vol. 203, no. 2, pp. 415-418, 2010.

[50] X. Xu and C. Cao, “Structure and ferromagnetic properties of Co-doped ZnO powders,” *Journal of Magnetism and Magnetic Materials*, vol. 321, no. 14, pp. 2216-2219, 2009.

[51] M. Zheng and J. Wu, “One-step synthesis of nitrogen-doped ZnO nanocrystallites and their properties,” *Applied Surface Science*, vol. 255, no. 11, pp. 5656-5661, 2009.

[52] J. Li, H. Fan, X. Chen, and Z. Cao, “Structural and photoluminescence of Mn-doped ZnO single-crystalline nanorods grown via solvothermal method,” *Colloids*

and Surfaces A: Physicochemical and Engineering Aspects, vol. 349, no. 1-3, pp. 202-206, 2009.

[53] B. Wang, M. J. Callahan, C. Xu, L. O. Bouthillette, N. C. Giles, and D. F. Bliss, "Hydrothermal growth and characterization of indium-doped-conducting ZnO crystals," *Journal of Crystal Growth*, vol. 304, no. 1, pp. 73-79, 2007.

[54] D. W. Zeng, C. S. Xie, B. L. Zhu, W. L. Song, and a. H. Wang, "Synthesis and characteristics of Sb-doped ZnO nanoparticles," *Materials Science and Engineering: B*, vol. 104, no. 1-2, pp. 68-72, 2003.

[55] D. Jung, "Syntheses and characterizations of transition metal-doped ZnO," *Solid State Sciences*, vol. 12, no. 4, pp. 466-470, 2010.

[56] Z. Zhang et al., "Cu-Doped ZnO Nanoneedles and Nanonails: Morphological Evolution and Physical Properties," *Society*, pp. 9579-9585, 2008.

[57] K. Kanade et al., "Self-assembled aligned Cu doped ZnO nanoparticles for photocatalytic hydrogen production under visible light irradiation," *Materials Chemistry and Physics*, vol. 102, no. 1, pp. 98-104, 2007.

[58] M. G. W. Frank J. Berry, John G. Dillard, Eric Faulques, Richard E. Russo, Gary J.Long, Fernande Grandjean, Lisa C. Klein, Shu-Fang Ho, Sung-Pirg Szu, Martha Greenblatt, Dale L. Perry, Walter H. Waddell, *Applications of Analytical*

Techniques to the characterization of Materials, First. A Division of Plenum Publishing corporatioin, 1991, pp. 41-57.

[59] B. D. CULLTY, *Elements of X-Ray Diffraction*, SECOND. ADDISON – WESLEY PUBLISHING COMPANY, INC, 1978, pp. 80-106.

[60] J. Hays et al., "Effect of Co doping on the structural, optical and magnetic properties of ZnO nanoparticles.," *Journal of physics. Condensed matter: an Institute of Physics journal*, vol. 19, no. 26, p. 266203, 2007.

[61] http://www.chem.qmul.ac.uk/surfaces/scc/scat5_3.htm 2012/02/20.

[62] J. C. RIVIÈRE, *Surface Analytical Techniques*, First. Oxford University Press, 1990, pp. 27-80 and 238-247.

[63] "http://www.lpm.u-nancy.fr/nanomag/spip.php?article192&lang=en 2012/02/20," 2012.

[64] "www.sem.com/analytic/sem.htm," *Scanning*.

[65] "http://infohost.nmt.edu/~mtls/instruments/Fesem/FESEM%20principle.htm." .

[66] Dr. HEINZ-HELMUT PERKAMPUS, *UV-VIS Spectroscopy and its Application*, First. Springer-Verlag Berlin Heidelberg, 1992, pp. 3-100.

[67] U. Pal, "Use of diffuse reflectance spectroscopy for optical characterization of un-supported nanostructures," *Spectroscopy*, vol. 53, no. 5, pp. 18-22, 2007.

[68] W. F. Stickle, P. E. Sobol, and J. Chastain, *Handbook of X-rays Photoelectron Spectroscopy*. Perkin-Elmer corporation, 1992.

[69] P. Suresh Kumar, J. Sundaramurthy, D. Mangalaraj, D. Nataraj, D. Rajarathnam, and M. P. Srinivasan, "Enhanced super-hydrophobic and switching behavior of ZnO nanostructured surfaces prepared by simple solution--immersion successive ionic layer adsorption and reaction process.," *Journal of colloid and interface science*, vol. 363, no. 1, pp. 51-8, 2011.

[70] H. Xue, Y. Chen, X. L. Xu, G. H. Zhang, H. Zhang, and S. Y. Ma, "X-ray diffraction spectroscopy and X-ray photoelectron spectroscopy studies of Cu-doped ZnO films," *Physica E: Low-dimensional Systems and Nanostructures*, vol. 41, no. 5, pp. 788-791, 2009.

[71] M. Caglar and F. Yakuphanoglu, "Applied Surface Science Structural and optical properties of copper doped ZnO films derived by sol – gel," *Applied Surface Science*, vol. 258, no. 7, pp. 3039-3044, 2012.

[72] S. Lee et al., "Effects of synthesis temperature on particle size/shape and photoluminescence characteristics of ZnS:Cu nanocrystals," *Materials Letters*, vol. 58, no. 3-4, pp. 342-346, 2004.

[73] L. Ma, S. Ma, H. Chen, X. Ai, and X. Huang, "Microstructures and optical properties of Cu-doped ZnO films prepared by radio frequency reactive

magnetron sputtering," *Applied Surface Science*, vol. 257, no. 23, pp. 10036-10041, 2011.

[74] M. Pashchanka et al., "A molecular approach to Cu doped ZnO nanorods with tunable dopant content.," *Dalton transactions (Cambridge, England: 2003)*, vol. 40, no. 16, pp. 4307-14, 2011.

[75] H. Liu et al., "The structure and magnetic properties of Cu-doped ZnO prepared by sol–gel method," *Applied Surface Science*, vol. 256, no. 13, pp. 4162-4165, 2010.

[76] N. Bouropoulos, I. Tsiaoussis, P. Poulopoulos, P. Roditis, and S. Baskoutas, "ZnO controllable sized quantum dots produced by polyol method: An experimental and theoretical study," *Materials Letters*, vol. 62, no. 20, pp. 3533-3535, 2008.

[77] M. Sahu and P. Biswas, "Single-step processing of copper-doped titania nanomaterials in a flame aerosol reactor.," *Nanoscale research letters*, vol. 6, no. 1, p. 441, 2011.

[78] H. Yang, S. Yu, S. Lau, T. Herng, and M. Tanemura, "Ultraviolet Laser Action in Ferromagnetic Zn1-xFexO Nanoneedles.," *Nanoscale research letters*, vol. 5, no. 1, pp. 247-51, 2009.

[79] N. Islam, T. B. Ghosh, K. L. Chopra, and H. N. Acharya, "XPS and X-ray diffraction studies of aluminum-doped zinc oxide transparent conducting films," *Analysis*, vol. 280, pp. 20-25, 1996.

[80] M. Chen et al., “X-ray photoelectron spectroscopy and Auger electron spectroscopy studies of Al-doped ZnO films,” *Applied Surface Science*, vol. 158, no. 1-2, pp. 134-140, 2000.

VITA

- **Name:** Esam Gunaid Abdo Al-Nahari
- **Place and date of birth:** Dhamar, Yemen, 1975
- **Address:** Physics Department, King Fahd University of Petroleum & Minerals, Dhahran 31261, Saudi Arabia.
- **Email :** isamesc2000@gmail.com

- **Nationality:** Yemen
- **Religion:** Muslim
- **Education:**
  - Bachelor of Education in Physics from Hodeidah University, Yemen, 1998.
  - Master student at Physics Department, King Fahd University of Petroleum & Minerals, Saudi Arabia.
- **Conference Publication:**
  - **Esam Gunaid AL-Nahari**, Synthesis and Characterization of Zinc Oxide (ZnO) Doped with Copper (Cu) by Microwave-assisted Polyol Method, Third Scientific Conference, Khobar, Saudi Arabia, (30 April - 03 May) 2012.
- **Position held:**
  - Graduate assistant at Physics department, Hodeidah University, Yemen, (1999- 2006).